Rare-Earth-Doped GaN: Growth, Properties, and Fabrication of Electroluminescent Devices

Andrew J. Steckl, *Fellow, IEEE*, Jason C. Heikenfeld, *Student Member, IEEE*, Dong-Seon Lee, *Student Member, IEEE*, Michael J. Garter, Christopher C. Baker, *Student Member, IEEE*, Yongqiang Wang, and Robert Jones

Invited Paper

Abstract—A review is presented of the fabrication, operation, and applications of rare-earth-doped GaN electroluminescent devices (ELDs). GaN:RE ELDs emit light due to impact excitation of the rare earth (RE) ions by hot carriers followed by radiative RE relaxation. By appropriately choosing the RE dopant, narrow linewidth emission can be obtained at selected wavelengths from the ultraviolet to the infrared. The deposition of GaN:RE layers is carried out by solid-source molecular beam epitaxy, and a plasma N_2 source. Growth mechanisms and optimization of the GaN layers for RE emission are discussed based on RE concentration, growth temperature, and V/III ratio. The fabrication processes and electrical models for both dc- and ac-biased devices are discussed, along with techniques for multicolor integration. Visible emission at red, green, and blue wavelengths from GaN doped with Eu, Er, and Tm has led to the development of flat-panel display (FPD) devices. The brightness characteristics of thick dielectric EL (TDEL) display devices are reviewed as a function of bias, frequency, and time. High contrast TDEL devices using a black dielectric are presented. The fabrication and operation of FPD prototypes are described. Infrared emission at 1.5 μm from GaN:Er ELDs has been applied to optical telecommunications devices. The fabrication of GaN channel waveguides by inductively coupled plasma etching is also reviewed, along with waveguide optical characterization.

Index Terms—Channel waveguides, electroluminescent devices, flat-panel displays, gallium nitride, molecular beam epitaxy, optical telecommunications, rare earths.

I. INTRODUCTION

MANY LANTHANIDE elements have played an important role in various optoelectronic and photonic applications [1], ranging from emitting elements in solid-state lasers (for example the Nd:YAG laser) and in phosphors for color lamps and displays (for example Eu and Tb) to optical fiber telecommunications (using Er or Pr). These so-called "rare earth" (RE) elements have a partially filled inner ($4f^n$) shell shielded from its surroundings by completely filled outer ($5s^2$ and $5p^6$) orbitals. Due to this shielding, the intra $4f^n$ shell transitions result in very sharp optical emissions at wavelengths from the ultraviolet to the infrared (IR). The wavelengths of these emission lines are determined by the energy of the transition between 4f states of the RE and are relatively independent of the host material. However, the host material does have a very strong effect on the radiative transition probability, in other words on the photoemission intensity. In general, RE-doped conventional semiconductors (Si, GaAs, etc.) have exhibited limited photoemission at room temperature due low RE solubility and severe temperature quenching. It was shown by Favennec *et al.* [2] that the thermal quenching in Er-doped semiconductors decreases with increasing bandgap. Therefore, wide-bandgap semiconductors (WBGS) are attractive hosts for RE elements.

The breakthroughs made with the incorporation of trivalent rare earth (RE^{3+}) elements into GaN films were previously briefly reviewed [3]–[5]. In this paper, we review in some detail the fabrication, properties, and application of RE-doped GaN electroluminescent devices (ELDs). As will be discussed in more detail, ELDs are optoelectronic devices operating [6] under high electric fields in order to generate hot carriers which, in turn, can impact-excite RE dopants and produce emission of light through RE radiative relaxation. GaN is a wide-bandgap semiconductor that is intensely investigated [7] for (intrinsic) optical and electronic applications. Er^{3+} doping of GaN has been shown [8] to produce strong near-IR 1.5-μm emission suitable for fiber-optic telecommunications from the lowest excited state. We have also obtained (for the first time) photoemission from higher excited RE states in GaN covering the entire visible spectrum: light emission in the green [9]–[11] (from Er at 537/558 nm), red [12], [13] (Pr at 650 nm, Eu at 621 nm), and blue [14] (Tm at 477 nm). Emission in the near-infrared (IR) is also obtained at 801 nm from Tm [14], at 1000 and 1540 nm from Er [11], and at 956, 1303, and 1914 nm from Pr [12]. The RE doping of GaN (as well as AlN and GaN) can be accomplished by ion implantation or by *in situ* doping during growth. Ion implantation has the advantage of a simple process and can control the doping concentration independent of the growth conditions. Many of the early reports [8], [15]–[19] on GaN:RE properties utilized ion implantation doping. However, the implantation doping approach also has disadvantages: introduction of damage in the GaN (which cannot be completely removed by annealing, especially at the higher concentrations used in ELDs), and the inability to uniformly dope thick layers (because of the limited penetration range of the heavy RE ions).
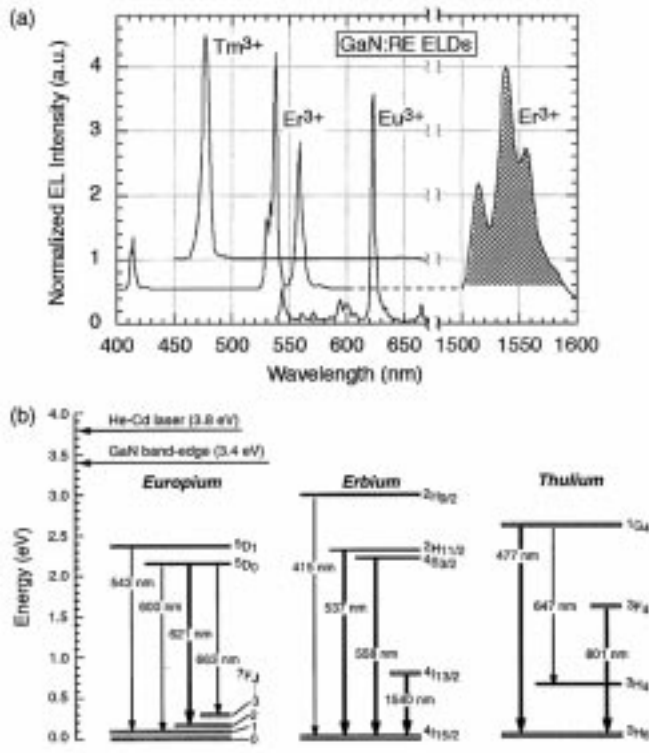
Fig. 1. RE-doped GaN photoemission: (a) emission spectra from Tm-, Er-, and Eu-doped GaN ELDs; (b) inner shell (intra-$4f^n$) transitions in Eu, Er, and Tm ions and corresponding emission wavelengths; also shown is the GaN bandgap energy and the laser (He–Cd) photon energy used for above-bandgap photo-pumping.

In situ RE doping requires a good understanding and control of the overall growth process and of the interaction of the RE flux with the main V/III fluxes. However, once that is established, good control of the RE concentration over many orders of magnitude can be obtained and very uniform doping can be accomplished. Furthermore, *in situ* doping does not suffer from the damage effects of ion implantation and, hence, results in more efficient emission [20]. In this paper, we restrict ourselves to REs introduced during growth of the GaN layer by molecular beam epitaxy (MBE). The substrates used for growth were sapphire, Si, and glass.

Emission spectra from GaN ELDs doped with Tm, Er, and Eu shown in Fig. 1(a) exhibit dominant visible emission lines at blue, green, and red wavelengths, respectively. IR emission at ~1.5 μm from the GaN:Er ELD is also shown. By comparison, the intrinsic emission from undoped GaN occurs in the ultraviolet part of the spectrum at ~365 nm, corresponding to a bandgap 3.4 eV. The primary visible colors emitted by GaN ELDs doped with these individual REs are very "pure" and match well the CIE coordinates adopted by the United States National Television System Committee (NTSC) and the European Broadcasting Union (EBU). In addition to the pure colors, mixed colors have been obtained by codoping GaN films with a combination of REs. GaN:RE ELDs have been developed which emit in a variety of pure and mixed colors. The electroluminescence (EL) emission is quite strong, being easily observable with the naked eye at room temperature. Thermal quenching of the emitted light is frequently not observed until well above

room temperature. Thus, RE doping of GaN represents an interesting alternative to semiconductor alloying (GaN/InN/AlN) for visible light-emission applications and has the additional attractive aspect of strong IR emission for telecommunications and other applications.

Theoretically, RE intra-$4f^n$ atomic transitions are parity forbidden by the Laporte selection rule. RE ions incorporated into a partially ionic solid favor substitutional occupation of the cation site. In addition to RE incorporation, the cation site must provide an uneven ligand crystal field in order to relax the selection rule and increase the probability of intra-$4f^n$ transitions. These 4f-4f transitions, however, are still not fully allowed, resulting in excited state lifetimes of ~1 μs − 1 ms for RE-doped systems. In wurtzitic GaN, which has a significant component of ionic bonding, the RE^{3+} ions have strong optical activity levels, since they are generally substitutionally located on the Ga sublattice where the lack of inversion symmetry produces strong ligand fields, thereby increasing the 4f–4f transition probability. These substitutional RE dopants are, therefore, likely to be the optically active RE centers observed in GaN:RE. The specific 4f transitions and associated emission wavelengths in GaN doped with Eu, Er, and Tm are shown in Fig. 1(b). The dominant transitions producing visible emission are indicated with thicker lines.

A simple model of the GaN:RE crystal structure is shown in Fig. 2(a). A strongly bonded GaN lattice, in conjunction with substitutional incorporation allows [21] unusually high RE doping concentrations (up to ~3–5 at.%), while preserving the optical activation of RE dopants. By comparison, the use of RE^{3+}-doped II–VI semiconductors as emitters and phosphors suffers from a more weakly bonded lattice, and substitutional location of the RE^{3+} ions on the 2^+ cation sites, which generates additional defects due to lack of charge neutrality. Rutherford back scattering (RBS) channeling analysis [22] confirms that a great majority (~95%) of the Er ions occupy substitutional sites on the Ga sublattice even at relatively high concentrations of >1 at.%. The Er–N bond has been measured by EXAFS analysis [23] to be 2.17 Å, versus a Ga–N bond length of 1.95 Å. This unusually short Er-nearest neighbor bond length in GaN is thought to be due to two major factors: 1) the low four-fold coordination, compared for example to a 12-fold coordination in $ErSi_2$; 2) a more polar bond for Er–N than for Ga–N (due to electronegativity differences), which helps to energetically compensate for the Ga–Er size mismatch.

Light emission from GaN:RE has been demonstrated via photoluminescence (PL), cathodoluminescence (CL), and EL. The dominant mechanisms for excitation and subsequent relaxation of RE dopants in GaN are depicted in Fig. 2(b). In PL, electron–hole pairs are generated by above band-gap photon absorption, charge carrier generation is provided by a high energy electron beam in CL, and in EL, carrier injection occurs by the application of bias voltage to electrical contacts on the GaN layer. The charge carrier energy is transferred to the RE dopants by impact excitation of hot carriers or as a result of nearby electron–hole recombination. The REs then experience either nonradiative relaxation (through multiphonon emission and/or Auger electron excitation) or radiative relaxation. The latter mechanism is the desired outcome as it results in the photoemission utilized in ELDs. The relative strength of the radia-
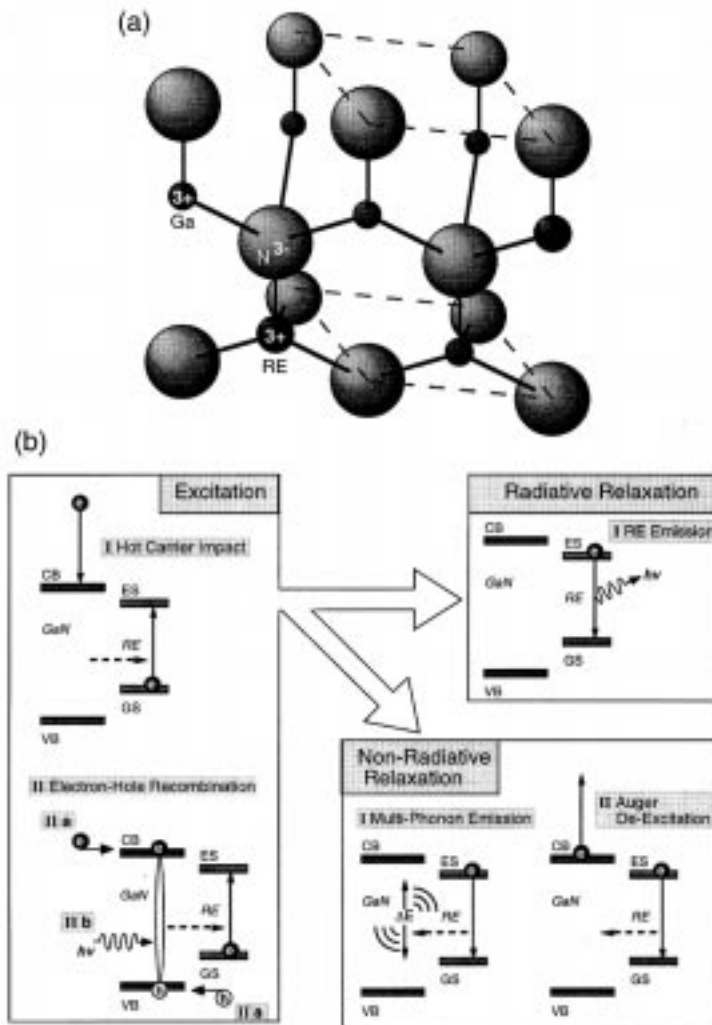
Fig. 2. Bonding and energy transfer mechanisms in RE-doped GaN: (a) bonding model for RE-doped GaN, with the RE^{3+} ion located substitutionally on the Ga sublattice; (b) mechanisms for RE dopant excitation and relaxation in the GaN host.

tive relaxation mechanism is a complex function of the GaN crystalline quality and the RE concentration. For example, increasing the crystallinity of the GaN host reduces the concentration of point defects, and thus reduces the opportunity for RE nonradiative relaxation. However, high crystallinity is normally achieved under conditions which prevent the incorporation of the optimum RE concentration into the GaN layer. Further, for the case of above-bandgap photo-pumping of highly crystalline RE-doped GaN, intrinsic (band-to-band) electron–hole recombination provides a high probability radiative intrinsic relaxation mechanism in competition with the RE radiative relaxation.

This paper is organized in four main sections. Section II discusses growth and optical properties of GaN:RE thin films, concentrating on the optimization of EL emission as a function of growth parameters (RE concentration, growth temperature, and N/Ga ratio). Section III covers the fabrication and characteristics of dc and ac devices as a function of operating temperature (dc) and time (ac), bias voltage (dc, ac) and frequency (ac). Section IV describes the application of GaN:RE ELDs to flat-panel display (FPD) devices. Discussion in Section IV also includes

high contrast devices, multicolor integration and the fabrication of FPD prototypes. Finally, Section V is concerned with the use of GaN:Er devices for 1.5-μm-based optical telecommunications.

II. GROWTH AND PROPERTIES

A. Overview of In Situ Doping During MBE Growth

As discussed in Section I, *in situ* RE doping of GaN has resulted in the successful fabrication of ELDs with red, green, and blue (RGB) color emissions using Eu, Er, and Tm, respectively. We have also achieved [24] RGB colors in EL emission from GaN:RE films grown at nominally room-temperature using the same set of RE elements. We have utilized MBE and *in situ* doping during growth for the deposition of GaN:RE thin films. With the exception of a plasma N_2 source, all other species were generated with elemental solid sources. Through detailed studies with GaN:RE ELDs, we have reached the understanding that the following are the most crucial factors for obtaining and improving EL emissions: RE concentration, growth temperature, and stoichiometry (i.e., V/III ratio) of the host material.

While our conclusions are derived from the solid-source MBE thin film growth, we believe that the same underlying principles would apply to other deposition techniques.

With regard to concentration, the EL emission increases more or less linearly with RE concentration at low levels. On the other hand, at high concentration levels, an emission quenching effect occurs due to an increase in RE–RE energy transfer, rather than radiative relaxation. Hence, there is an optimum RE concentration for which maximum emission is observed. Most phosphor systems exhibit this concentration quenching phenomenon. For example, ZnS:Mn exhibits [25] its luminance maximum at 0.5–1.0 wt.% of Mn. Growth temperature and Ga flux (V/III ratio) affect the RE emission through the properties of the GaN host (such as crystallinity and resistivity) and directly through their influence on RE incorporation. These three parameters, RE flux (determined by the RE cell temperature), growth (substrate) temperature, and Ga flux (determined by the Ga cell temperature) are externally controlled and adjusted during GaN:RE MBE growth. Through this optimization we can gain a better understanding of the real mechanisms behind many of the unique optical and electrical properties of GaN:RE ELDs. Moreover, this optimization process has led to improved devices being fabricated for various applications.

The optimization experiments have concentrated on dc Er-doped GaN grown on Si substrates in a Riber 32 MBE system. A typical MBE growth cycle starts with a p-type (111) Si substrate preheated at 500 °C in the preparation chamber and outgassed at 850 °C for 10 min in the growth chamber. Electron diffraction shows clear 7×7 reconstruction patterns on the Si (111) surface after outgassing. A thin film of AlN (or GaN) is first grown for 2–5 min as a buffer followed by GaN:Er growth for 1 h. For dc-EL measurements, a simple ring-shaped Schottky electrode is fabricated [26] on top of the GaN:Er film using indium–tin oxide (ITO) sputtering and a liftoff process. The electrode has an area of 7.65×10^{-4} cm^2; its detailed structure is discussed in Section III-A.

Devices designed for display operation incorporate GaN films grown on dielectric layers and are operated in the ac mode. The quality of GaN grown on amorphous dielectric layers is certainly not as high as that of GaN grown on crystalline (sapphire or Si) substrates. However, the quality is still fairly high and certainly sufficient for the operation of ac-ELDs. For example, we have previously reported [46] that GaN grown on sputtered Al$_2$O$_3$ layers exhibited an X-ray peak with a surprisingly narrow linewidth of 0.174 °.

B. Optimizing the RE Concentration

We have observed [27] that the visible and IR emission, from both PL and EL, are a strong function of Er concentration. In general, all Er-doped host materials exhibit a practical limit in Er concentration beyond which the optical emission begins to decrease. The ultimate doping limit is the RE solid solubility in the host material. Concentrations which are introduced in a nonequilibrium process and which are larger than the solid solubility can result in the formation of a second phase material which contains some (or all) of the RE concentration. This precipitation is accompanied by the concomitant degradation of op-
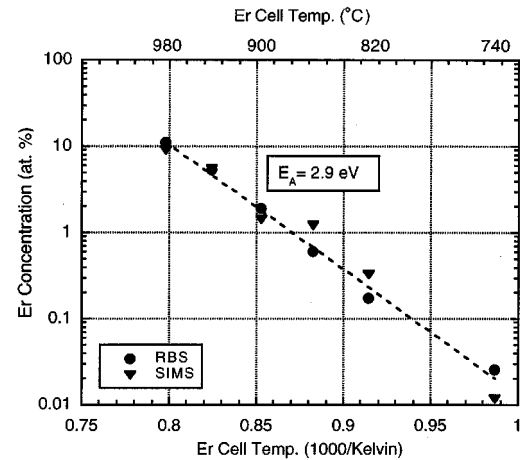

Fig. 3. Er concentration in GaN as measured by RBS and SIMS as a function of Er cell temperature. The measured activation energy of 2.9 eV is in close agreement with the value of ~3.0 eV for the Er vapor pressure temperature dependence.

tical and electronic properties of the host material. A practical limit, which is usually reached first, has to do with the concentration quenching effect discussed in Sections I and II-A. For example, the solubility limit of Er in Si is ~10^{18} cm^{-3}, while the PL intensity at 1.54 μm was reported [28] to saturate at even lower concentration of ~5×10^{17} cm^{-3}, which represents an Er atomic percentage of only ~10^{-3} at.%. Other reported maximum Er concentrations include ~5×10^{18} cm^{-3} in GaAs [29] and 4×10^{19} cm^{-3} in Al$_2$O$_3$ [30].

RBS and secondary ion mass spectroscopy (SIMS) measurements were used to measure absolute Er concentrations in GaN:Er films. Measurement results showed that the Er concentration in GaN ranged from 0.025 to >10 at.% by varying the Er cell temperature from 740 °C to 980 °C, as shown in Fig. 3. The Er concentration follows an exponential dependence on the Er cell temperature. An Arrhenius-like thermal activation energy estimated from this curve was 2.9 eV, which gives an excellent agreement with the activation energy of ~3.0 eV for the Er vapor pressure in this temperature range [31].

PL was performed at room temperature both in the visible and infrared regions by above-bandgap excitation with a 325-nm He–Cd laser. Visible and IR PL intensities are plotted in Fig. 4(a). Green emission at 537 nm is one of the characteristic emissions due to 4f-4f inner shell transition of Er^{3+} ion and is attributed to a transition from ^{2}H$_{11/2}$ to ^{4}I$_{15/2}$ [see Fig. 1(b)]. IR emission at 1.54 μm is a well-known transition from ^{4}I$_{13/2}$ to ^{4}I$_{15/2}$ and has special importance in optical communication applications. As shown in Fig. 4(a), both of these emissions have maxima at about 1 at.% Er. It is well known in phosphor materials [32] that the optical excitation intensity of RE ions exhibits an optimum concentration. As the RE ion concentration is increased, the average distance between ions is reduced proportional to the cube root of the RE concentration. When RE ions are located sufficiently close to each other, the excitation residing in one ion can migrate to a neighboring ion of the same species as a result of resonant energy transfer. This process is known as cross-relaxation. The energy migration process increases the possibility that
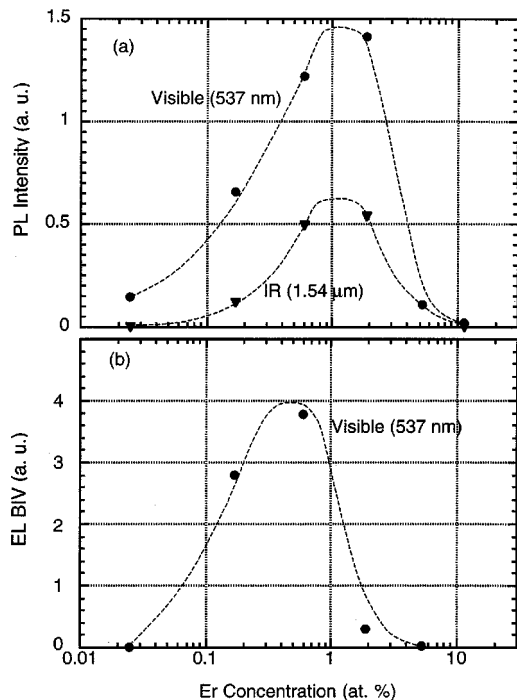
Fig. 4. Photoemission intensity as a function of Er concentration: (a) visible and IR PL intensity display a common maximum at ∼1 at.% Er; (b) visible EL intensity normalized by current flow (BIV) shows a maximum at ∼0.5 at.% Er.

the excitation is dissipated at nonradiative sites, resulting in a saturation or a decrease in optical emission.

Brightness normalized by current flow, defined as BIV, is plotted in Fig. 4(b) for devices with various Er concentrations. Since the EL brightness is influenced by many factors, including sample conductivity and device fabrication effects, the current-normalized brightness is a more appropriate parameter to evaluate rather than the "raw" brightness (i.e., brightness regardless of current flow through the device at a fixed applied voltage). The optimum Er concentration is 0.5–1 at.% for visible EL emission, which is almost the same as that observed in PL. Combining this with the results of visible PL lifetime and XRD previously reported [27], we conclude that the optimum Er concentration is ∼1 at.%. The corresponding Er–Er spacing is estimated to be ∼15 Å.

C. Optimizing the Growth Temperature

Experiments designed to determine the optimum growth temperature for GaN:Er films were carried out at temperatures ranging from 100 °C to 750 °C. The Er cell temperature was fixed at 860 °C. Interestingly, all films exhibited EL regardless of growth temperature. The maximum BIV (i.e., the largest current-normalized brightness obtained over the current-voltage range measured in each case) for each device is plotted in Fig. 5. Starting at low growth temperature, BIV increases nearly exponentially with growth temperature, exhibits a maximum at ∼600 °C and decreases at higher temperatures. This is the same trend as obtained [33] from the PL data and from structural characterization, reinforcing the conclusion that 600 °C is the optimum growth temperature for visible emission from GaN:Er.
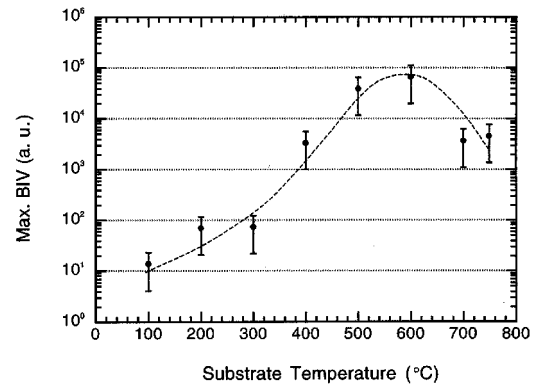

Fig. 5. Maximum current-normalized EL brightness (BIV) as a function of growth temperature. BIV experiences a maximum at 600 °C.

Electroluminescence in GaN:Er devices is obtained by carrier impact excitation. To accelerate injected electrons to a sufficient energy requires high electric fields. In turn, to reach the needed electric fields requires relatively resistive samples. The devices fabricated from the film grown at 600 °C were the most resistive and showed strongest EL emission. As a result, they produced the highest maximum BIV. Decreased BIV from films grown at 700 °C and 750 °C is due mainly to the more conductive nature of those films, in spite of comparable raw EL intensity. We believe that the main cause for the increased conductivity of these films has to do with their rough morphology which allows for many electrical leakage paths.

We conclude that an MBE growth temperature in the neighborhood of 600 °C produces the optimum ELD emission intensity.

D. Effect of V/III Ratio

RE optical emission from GaN films is a strong function of the ratio of the Ga- and N-bearing fluxes (V/III) during growth. The V/III ratio can be modified by changing either component, but is typically adjusted by controlling the Ga flux. The Ga flux is critical to GaN crystalline quality and good crystalline GaN is usually grown under slightly Ga-rich [34] growth conditions. GaN crystallinity and intrinsic luminescence are strong functions of Ga flux during growth. Therefore, it is clear that the RE-related emission, which is dependent on the crystallinity of the GaN host, will also be strongly affected by the Ga flux.

Er-doped GaN films were grown with various Ga cell temperatures from 850 °C to 945 °C, resulting in beam equivalent pressures (BEP) from ∼1.5×10^{-7} to ∼9.0×10^{-7} torr. All other growth parameters were fixed at 600 °C for growth temperature and 860 °C for Er cell temperature.

GaN:Er film thickness achieved in 1-h growth is plotted in Fig. 6(a) versus Ga flux specified by BEP in the MBE system. The film thickness increases with Ga flux up to ∼5×10^{-7} torr. This is the Ga-controlled (or N-rich) growth regime, wherein increasing the Ga availability increases the rate at which the Ga–N reaction proceeds. At Ga fluxes beyond 5×10^{-7} torr, the growth rate is constant at ∼0.5 μm/h. This is the Ga-rich growth regime, wherein we have saturated the ability of the reaction to consume Ga (at the given growth temperature and N flux). The V/III ratio which results in the stoichiometric growth condition
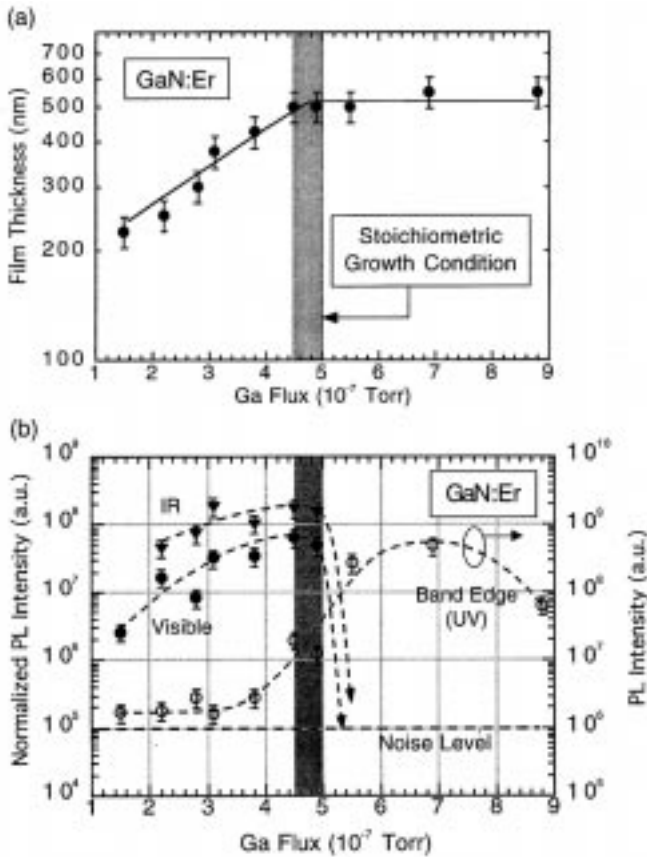
Fig. 6. Effect of Ga flux on GaN growth rate and GaN:Er PL: (a) GaN:Er film thickness versus Ga flux used during growth. The stoichiometric growth condition was determined by film thickness saturation to be between $\sim4.5 \times 10^{-7}$ and $\sim5.0 \times 10^{-7}$ torr in Ga beam equivalent pressure; (b) PL intensity from GaN:Er films versus Ga flux. GaN band-edge emission at 369 nm increases with Ga flux and has a maximum in the Ga-rich growth regime; the PL intensity of visible and IR emission from Er^{3+} ions (normalized by the incorporated Er concentration) increases with Ga flux and then drops abruptly to the detection limit near the stoichiometric growth condition.

is determined [35] as the Ga flux at the onset of thickness (or equivalent growth rate) saturation. In this set of samples, stoichiometry occurs for Ga flux between 4.5×10^{-7} and 5.0×10^{-7} torr (shaded region in the plot).

Fig. 6(b) shows the visible and IR PL intensity as a function of Ga flux. Above GaN bandgap excitation with the He–Cd laser (325 nm) was utilized in order to observe emission from Er^{3+} ions, as well as UV band-edge emission of the GaN host. Visible and IR data were normalized to the incorporated Er concentration in each sample. The GaN band-edge emission at 369 nm was much stronger in samples grown under Ga-rich conditions, consistent with the results of other groups. Reduced intensity at the highest Ga flux is due to Ga droplets formed on the GaN surface, which act as a screen for the emitted light. The PL from Er^{3+} ions exhibits a very interesting behavior. Both visible and IR emission increased with Ga flux up to the stoichiometric growth condition followed by a very abrupt emission reduction, to the detection limit of the measurement. EL emission exhibited [35] the same trend. Under the above-bandgap PL excitation, the quenching of the Er-based emission near the stoichiometric growth condition is probably due to the increasing efficiency of the intrinsic band-edge emission in the GaN host,
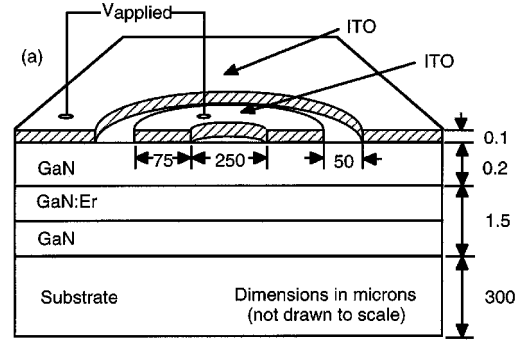

Fig. 7. Cross-section schematic of the GaN:RE dc-ELD structure, consisting of GaN undoped and RE-doped layers and transparent indium–tin oxide electrodes. Due to electrode size, the larger ITO electrode is essentially ohmic, whereas the small ring electrode is rectifying.

which then provides a faster relaxation path for excited carriers. Under EL excitation, increased GaN conductivity reduces the allowable applied field and resulting hot carrier energy for impact excitation.

We conclude that the optimum growth condition for Er optical activity is found under slightly N-rich flux near the stoichiometric region. Under these growth conditions, the resulting GaN crystallinity is high enough for efficient Er excitation but the competition from intrinsic carrier recombination is not yet very strong. Furthermore, the higher resistivity of GaN grown under slightly N-rich conditions is favorable for supporting high electric fields for hot carrier generation.

III. GaN:RE ELD FABRICATION AND CHARACTERIZATION

Both dc- and ac-ELDs were investigated. DC-ELDs involve fewer fabrication steps as they do not require insulating layers, can be grown directly on crystalline substrates (either Si or sapphire), and only require the deposition of a transparent electrode. On the other hand, ac-ELDs are much more robust, efficient, and have a much longer lifetime. Therefore, the ac structure is used in ELD-based FPDs. DC ELDs were utilized in basic studies of the growth conditions (as discussed in Section II) and in device temperature-dependence investigation (discussed in Section III-A). Brightness, lifetime and other FPD-related device characteristics were investigated using ac-ELDs (discussed in Section III-B).

A. DC Devices

A schematic cross section of the GaN:Er ELD is shown in Fig. 7. A small circular inner electrode is separated from a much larger outer electrode, which surrounds it. Visible and IR emission is present during positive and negative bias, but intensity is much greater under the negatively biased electrode. This is likely due to the fact that there is avalanche breakdown occurring under the reverse biased electrode, thus providing a large concentration of "hot" electrons. The breakdown voltage decreases with increasing temperature, which has been shown to be related to the presence of defects [36] in similar materials. There is almost no emission from the region of material between electrodes.
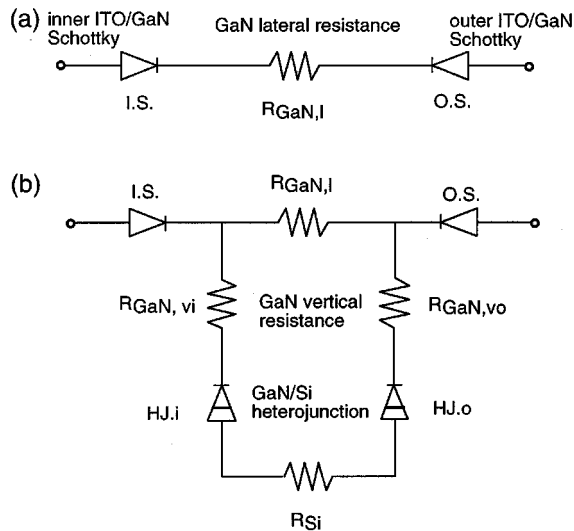
Fig. 8. Equivalent circuit models for the GaN:RE dc-ELD: (a) insulating (sapphire) substrate; (b) semiconducting (Si) substrate.

Fig. 9. Temperature dependence of EL emission from GaN:Er dc-ELDs: (a) visible emission at 537, 558, and 666 nm; (b) infrared emission at 1.5 μm.

The choice of ITO as both the emitting and ground contact was made for reasons of convenience. Using ITO for both electrodes allowed for single mask device patterning. An additional advantage of using ITO is that it is relatively transparent in both the visible and infrared wavelengths. The conductivity of the ITO is also nearly independent of temperature. ITO has been used as a contact for both n-type [37] and p-type [38] GaN. However, GaN:Er is basically semi-insulating and we consider ITO to form a Schottky contact.

Fig. 8(a) shows a simple equivalent circuit model of dc devices on sapphire consisting of two back-to-back Schottky diodes representing the ITO/GaN electrodes and a resistor connecting them. Since sapphire is truly an electrical insulator, the entire current flow occurs through the GaN film. For either positive or negative bias, one Schottky diode is forward biased and one Schottky diode is reverse biased. The reverse-biased diode controls the flow of current initially. No current flows until a significant voltage is reached, at which point the reverse biased diode undergoes avalanche breakdown, resulting in carrier generation. Current now begins to flow through the forward biased diode. At this point, the resistor between the two diodes, representing the GaN:Er film, becomes the current limiting element of the device.

Fig. 8(b) is the equivalent circuit model for devices on Si. In this case, one allows for current flow through the semiconducting substrate with the addition of GaN–Si junctions. Notice that if charge flows through the lateral GaN resistor and through the Si, then the model can be reduced to that seen in Fig. 8(a), except the resistor becomes the series resistance of the entire device. The carrier transport of the resistor is somewhat complicated and is considered in more detail elsewhere [39].

Fig. 9(a) shows the temperature dependence of the EL peak intensity of the main Er visible emission lines at 537 and 556 nm, and of a minor peak at 666 nm. It is clear that over the temperature range from 230 K to 500 K each Er^{3+} electronic transition is excited differently as the temperature is varied. If the individual emission lines are summed, we observe that electrical
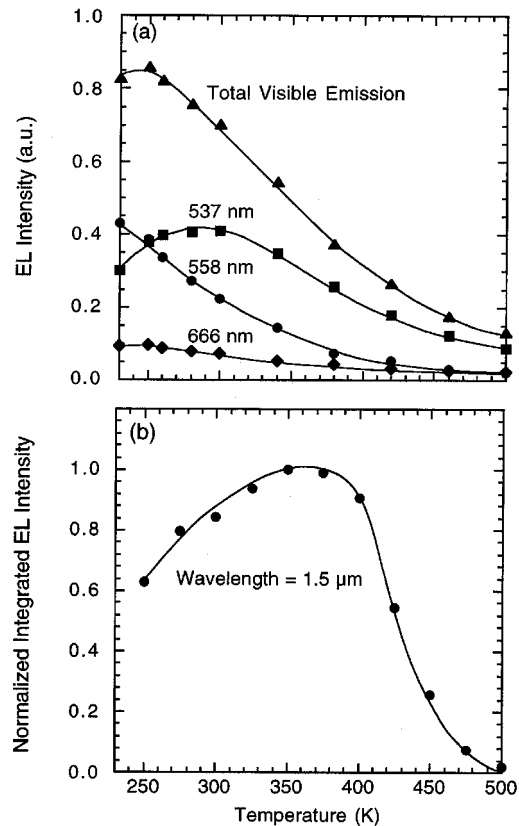
pumping produces the same temperature dependence first reported through the use of optical pumping [9]. Therefore, we can conclude that the temperature dependence of the visible emission intensity is solely a function of temperature and not the pumping method.

The temperature dependence of the 1.5-μm IR emission from a GaN:Er ELD is also shown in Fig. 9. The EL intensity reaches a peak above room temperature, at ~100 °C (375 K). Notice that at least 80% of the maximum IR emission is obtained for an operating temperature range of ~140 °C (from 270 K to 410 K). This is very useful for 1.5-μm erbium devices allowing great flexibility in terms of operating under extreme conditions, especially when considering the temperature dependence of the 1.5-μm Er emission in other semiconductor hosts (such as Si [40], [41], GaAs [42], and GaP [43]) which exhibit varying degrees of temperature quenching well below room temperature.

In this section, the temperature dependence of visible and IR rare-earth-activated electroluminescence in GaN:Er dc-ELDs was presented, along with a simple electrical model. The fact that the 1.5-μm emission does not exhibit thermal quenching in the vicinity of room temperature indicates the potential of GaN:Er technology for optical communication applications.

B. AC Devices

1) Device Structure: The form of electroluminescence utilized for operation of dc GaN:RE ELDs fits into the category of high-field (~MV/cm) electroluminescence. Organic-light

emitting diodes (OLED) are also an example of dc high-field electroluminescence technology. Reliable high-field dc operation requires structurally defect-free luminescent thin films. Irregularities in the film structure can result in high field points or electrical shorts which cause device failure through destructive electrical breakdown of the luminescent layer. For OLEDs, even slight irregularities in film structure can cause high field points, which then become the dominating mode of device degradation [44]. This thin-film uniformity requirement results in extreme fabrication difficulties for large area dc-ELDs and OLEDs. OLEDs inherently must be driven under dc high field conditions and cannot circumvent this stringent fabrication criterion. There is, however, an alternative bias scheme/device structure [45] available to inorganic-EL phosphors such as GaN:RE which allows reliable high-field operation of large area electroluminescence devices. This approach incorporates at least one insulating layer into the device structure converting it essentially into a capacitor and utilizes alternating current biasing. This ac-biased metal/dielectric/phosphor/dielectric/metal layered device (ac-ELD) allows reliable high field operation by current-limiting the electrical breakdown of the phosphor layer.

The ac-ELDs consist of a dielectric/GaN:RE/dielectric structure, shown schematically in Fig. 10(a). A variety of dielectrics have been investigated [46], ranging from low permittivity, thin-film dielectrics (such as SiO_2, Si_3N_4 or AlN—the latter forming an "all-nitride" structure), to very high-permittivity thick dielectric layers (such as $BaTiO_3$). In contrast to the GaN:RE dc-ELDs (see Fig. 7) which used epitaxial growth conditions on crystalline substrates and were operated under dc bias, these ac-ELDs are most often formed on amorphous substrates (glass) and are operated under bipolar ac bias.

A simple electrical equivalent circuit [47] of an ac-ELD is shown in Fig. 10(b). The dielectric layers are modeled as ideal capacitors, while the phosphor layer is modeled as a capacitor in parallel with two back-to-back diodes. In a dc-ELD, bias current increases with applied voltage (and, therefore, field) until catastrophic electrical breakdown of the GaN:RE phosphor layer occurs. In contrast, for an ac-ELD the maximum applied voltage is determined by the electrical insulating strength of the dielectric layers, which is greater than that of the phosphor. The turn-on voltage for light emission in an ac-ELD occurs when the phosphor layer is subjected to an electrical field beyond its electrical breakdown, thus allowing current flow. This is the case when the voltage applied across one of the reverse biased diodes on Fig. 10(b) is sufficient to achieve breakdown. The operational current in an ac-ELD above threshold is roughly proportional to the product of the bias frequency and the capacitance of the dielectric layers. As the polarity of the applied voltage is reversed, light is emitted as electrical charge carriers travel through the phosphor layer. The light emission pulses are then integrated by the human eye, resulting in device brightness values of 10–1000 cd/m^2. Unlike dc-ELDs, GaN:RE ac-ELDs inherently allow high-field biasing without reduced current saturation of the emission intensity. Most 4f-4f RE^{3+} emissions have long lifetimes since the RE^{3+} transitions are partially forbidden by the parity selection rule. Therefore, bipolar excitation (ac-biasing) at a frequency lower than the inverse of the emission lifetime is necessary in order to efficiently excite a GaN:RE
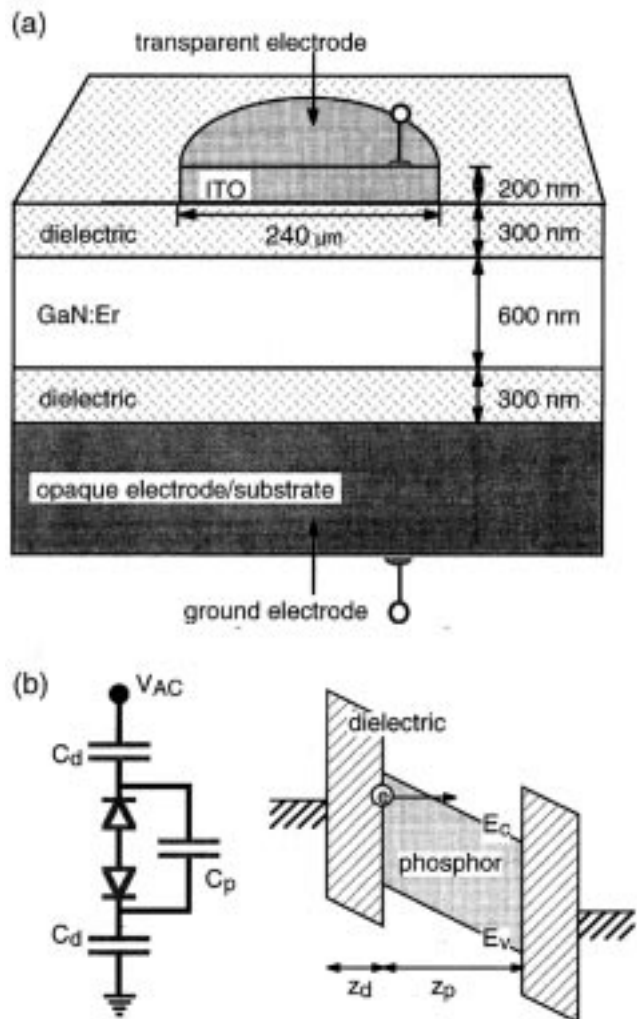

Fig. 10. The GaN:RE ac ELD: (a) cross-section schematic of a simple structure, consisting of a GaN:Er film sandwiched between two dielectric layers, the substrate as ground electrode if sufficiently conducting, and the transparent ITO top electrode; (b) equivalent circuit model and energy band diagram of a biased ac-ELD.

phosphor. The rise/fall time of the applied voltage is normally less than 1 ms, the spontaneous emission lifetime [48] for the RE is also normally less than 1 ms, resulting in efficient biasing up to 1 kHz or higher. For video rate displays, meeting the ∼100 Hz frame-rate requirement is easily achieved by ac-ELDs without the need for active matrix addressing which is required for much less responsive technologies such as liquid crystal displays (with time constants of tens of milliseconds).

2) Fabrication Techniques: As detailed in Fig. 11, the ac-ELD structures can be fabricated into an inverted structure (Fig. 11(a), light emission away from the substrate) or a traditional structure (Fig. 11(b), light emission through the substrate). The basic ac-ELD fabrication sequence involves similar thin-film requirements for the traditional and inverted device structures. The fabrication processes start with either p^+-Si substrates for the inverted structure or Corning 1737 aluminosilicate sheet glass for the traditional structure. Inverted devices have the advantage of potential Si integration, whereas the traditional devices can be scaled to much larger substrate

a) Inverted GaN:RE
AC-ELD Fabrication

| rear electrode / substrate
Si, metal, or metal coated glass |
| rear insulating dielectric
high capacitance oxide or nitride |
| light emitting phosphor
GaN:RE |
| front insulating dielectric
high capacitance oxide or nitride |
| front transparent electrode
In₂O₃:SnO₂ or ZnO:Al |

b) GaN:RE AC-ELD
Fabrication on Glass

| transparent substrate
hi-strain point sheet glass |
| front transparent electrode
In₂O₃:SnO₂ or ZnO:Al |
| front insulating dielectric
high capacitance oxide or nitride |
| light emitting phosphor
GaN:RE |
| rear insulating dielectric
high capacitance oxide or nitride |
| rear electrode
metal |

c) Process Steps For Inverted AC-ELD Fabrication

8) thick or thin film metal electrode
7) black pigmentation
6) thick film BaTiO₃ dielectric
screen printing and sintering
5) thin film dielectric sputtering
4) thin film GaN:RE phosphor
reactive evaporation
3) thin film dielectric sputtering
2) thin film In₂O₃:SnO₂
electrode sputtering
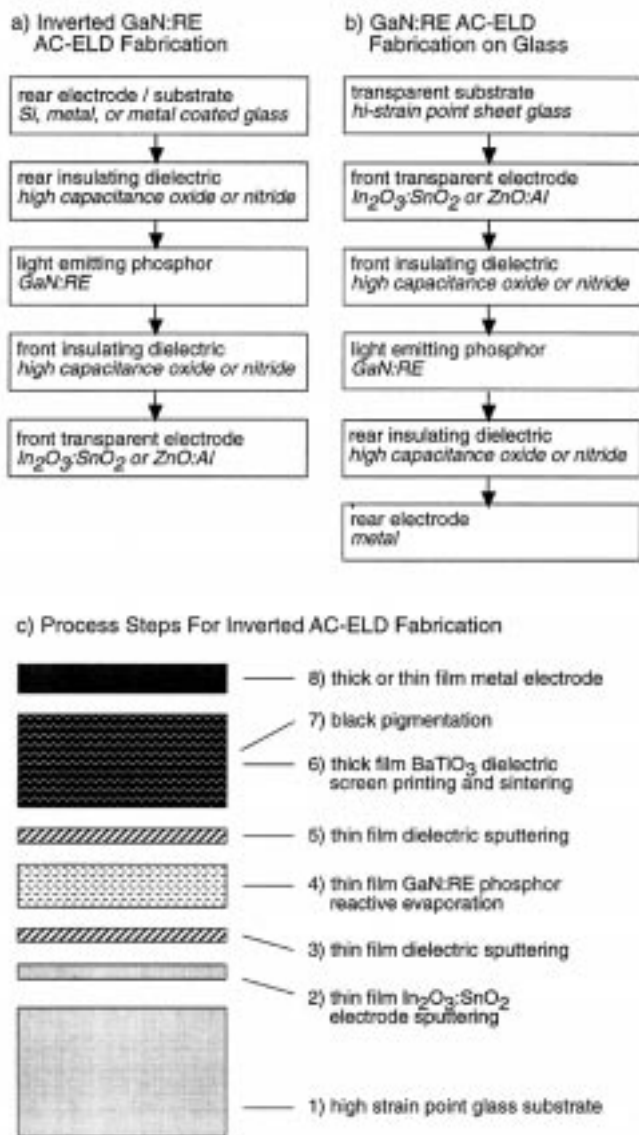1) high strain point glass substrate

Fig. 11. AC-ELD fabrication: fabrication steps for (a) inverted (opaque substrate) and (b) noninverted structures (transparent substrate); (c) schematic and process steps for the noninverted ELD structure.

Fig. 12. Brightness of a GaN:Eu ac-ELD operated at a frequency of 1 kHz as a function of: (a) voltage; (b) view angle.

sizes ($\sim$1 m^2 sheet glass). Dielectric layers can be sputter deposited and can be chosen from the set of Al$_2$O$_3$, AlN, Si$_3$N$_4$, SiON, BaTa$_2$O$_6$, BaTiO$_3$, and SrTiO$_3$. AlN, deposited by MBE, is often used as a insulator dielectric for GaN:RE ac-ELDs because it has the additional advantages of *in situ* deposition and use as buffer layer for promotion of GaN:RE grain growth. The GaN:RE layer thickness ranges from 0.5 to 1 μm and exhibits a permittivity of $\varepsilon_r \sim 8$. For the inverted thin-film dielectric structure (TFEL), the dielectric layer thickness ($>$200 nm) and permittivity ($\varepsilon_r > 8$) are such that the ac-ELDs operate reliably and the majority of applied voltage is capacitively coupled to the phosphor layer for efficient device operation. The deposition parameters of the GaN:RE phosphor are similar to those described in Section II. In the noninverted structure, the rear dielectric layer, adjacent to the opaque metal electrode, can also be formed as a thick film ($>$10 μm) by techniques such as screen-printing followed by sintering. The

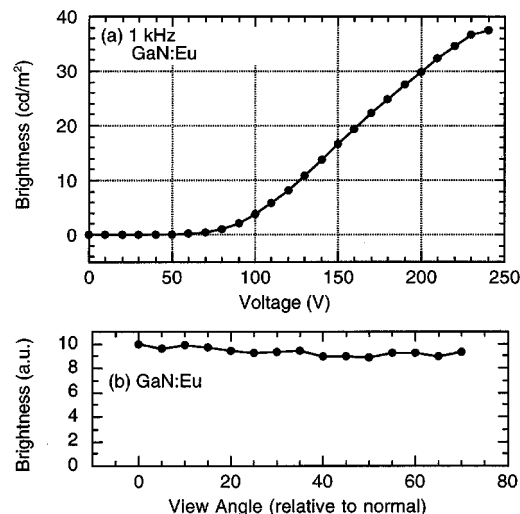details of novel GaN:RE thick-film dielectric ELDs (TDEL) are discussed in Section IV.

3) Characteristics: The luminance versus voltage characteristics for a TFEL ac-ELD with a $\sim$1-μm GaN:Eu phosphor layer is shown in Fig. 12. GaN:Eu TFEL ac-ELDs have shown maximum red luminance values of $\sim$40 cd/m^2 at 240 V$_p$ and 1 kHz square wave. It is important to note that ac-ELDs are high-voltage/low-current devices. Furthermore, unlike other high-field OLEDs, ac-ELDs are capable of generating very high peak luminance without device degradation. For example, a GaN:Er ac-ELD, which exhibits an average luminance of 20 cd/m^2 at 1-kHz bipolar bias, exhibits a peak luminance of $\sim$4000 cd/m^2. This value is calculated from the luminance per cycle per second (20 cd/m^2/1000 cycle $= 0.02$ cd/m^2 per cycle) divided by the approximate length of the light emission event ($\sim$5 μs for Er). The luminance threshold of $\sim$60 V is 100–200 V lower than the threshold voltage for devices utilizing sulfide- and oxide-based EL phosphors. Utilizing a thinner $\sim$500 nm GaN:Eu phosphor produces a luminance of $\sim$25 cd/m^2 at a bias voltage of 120 V. High-voltage ($\pm$200 V) complementary MOS drivers are readily available for biasing of large area ac-ELDs. The independence of brightness with view angle is seen in Fig. 12(b). The ability to have uniform emission over a wide range of view angles is one of the major advantages of emissive displays over liquid crystal displays.

GaN:Er ac-ELDs exhibit equally strong visible and IR emissions. The frequency dependence of visible (537/558 nm) and IR emission (1550 nm) from a GaN:Er TFEL ac-ELD is shown in Fig. 13. The infrared (1550 nm) GaN:Er emission originates from relaxation of the lowest excited Er^{3+} state (^{4}I$_{13/2}$). Its specific applicability to optical communications will be discussed later in Section V. At low frequency ($<$1 kHz), the expected linear relation between frequency and visible and IR emission intensity is observed, with roughly as many photons emitted in the IR as in the green. As the frequency increases beyond 1 kHz, there is a clear saturation of the IR intensity. The visible emission intensity also increases sublinearly with frequency, but at
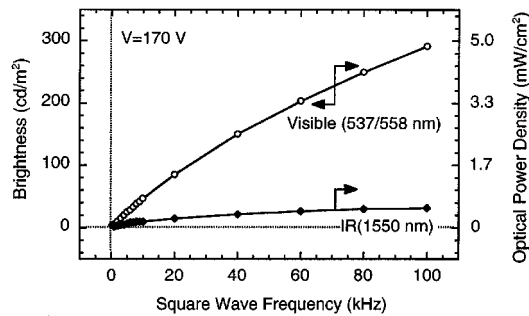
Fig. 13.   Brightness of a GaN:Er ac-ELD at 170 V as a function of drive frequency. Optical power density emitted in the visible (at 537/556 nm) and IR (at 1.5 μm) is also shown.
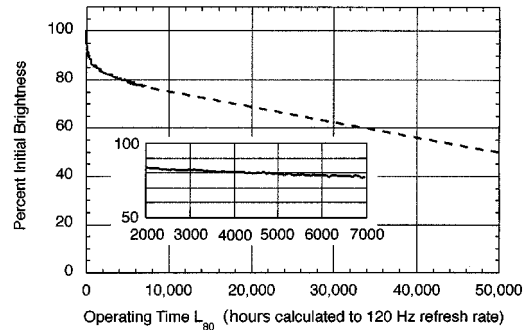

Fig. 14.   Brightness of GaN:Eu ac-ELD as a function of operating time. The device is biased at 80 V above threshold. Extrapolation of the brightness decrease in the linear regime indicates a device lifetime (defined as 50% of initial brightness) of 50 000 h.

higher frequencies. The frequency saturation is attributed to the GaN:Er excited state lifetime [48] of each particular transition. These lifetimes have been measured to be on the order of $\sim$10 μs for the visible green emission and $\sim$1 ms for the 1.5-μm IR emission. Similar results have been observed for GaN:Eu where an onset of frequency saturation for GaN:Eu red emission above 1 kHz confirms that the GaN:Eu emission lifetime is relatively long ($\sim$200 μs). Blue emitting GaN:Tm ac-ELDs behave similarly to GaN:Er ac-ELDs at high frequency since they also exhibit a relatively short spontaneous emission lifetime ($\sim$tens of microseconds).

One of the distinct advantages of GaN:RE EL phosphors is the rugged nature of the nitride material system. Unlike II–VI based ac-ELD phosphors and organic light emitting diodes, GaN:RE phosphors are stable at high temperatures and do not degrade when exposed to air/water. This allows for flexibility in device fabrication, low-cost device packaging, use in harsh environments, and very long lifetime operation. Previous attempts to bring about these advantages have focused on oxide ac-ELD phosphors. However, the highly-insulating oxide phosphors generally require much higher operating voltage than GaN:RE phosphors and there does not yet exist an efficient blue oxide phosphor to enable full-color operation. Nitride phosphors offer the same stability benefits of oxide phosphors without the high-voltage requirement. As shown in Fig. 14, nitride phosphors in a ac-ELD structure show excellent accelerated aging characteristics even without hermetic sealing. The lifetime data in Fig. 14 extrapolates to 50 000 h to reach 50% brightness for 120-Hz device operation. The device lifetime varies inversely with the bias frequency, since power is dissipated and light is emitted from the device only when the polarity of the bias voltage is reversed. Between excitations, there is no power dissipation and the GaN:RE phosphor and surrounding device structure do not deteriorate in brightness potential. The initial rapid luminance decrease is similar to that seen in other ELD devices and is due to permanent electrical breakdown at pinholes/defects in the phosphor layer [6]. These small breakdown points do not adversely effect long-term reliability of the device. In commercial ELD displays, this initial luminance decrease is removed by a high-frequency "burn-in" stage which then allows for the display operation to begin in the linear aging regime for improved gray-scale capability. It is reasonable to expect future improvements in GaN:RE ac-ELD

efficiency and reliability resulting in operational lifetimes of 50 000 to 100 000 h at frequencies as low as 60 Hz.

It is interesting to compare the total number of lumens that can be emitted from a GaN:RE ELD to an OLED display device. With improvements in luminous efficiency ($\sim$1 lm/W) of the GaN:RE phosphor layer the product of brightness ($\sim$100 cd/m^2) and operational lifetime at 50% luminance ($\sim$ 50 000 h) would result in a total luminance generation of $\sim$5 $\times$ 10^6 cd/m^2-h. This is an order of magnitude larger that that of a commercial OLED display which is capable of $\sim$5 $\times$ 10^5 cd/m^2-h ($\sim$100 cd/m^2, 5000 h).

IV. APPLICATIONS TO FPDs

A. Device Structures for High Contrast

A proven technology, ac-ELDs have provided the highest level of monochrome display reliability. Recent breakthroughs in phosphor research have led to filtered full-color ac-ELD displays [49]. However, the potential for low-cost and high-performance ac-ELD displays is limited by the need for color filtering of the broad spectrum emitting II–VI phosphors and by the stringent fabrication requirements for thin-film dielectrics. In order to remedy these limitations, we have developed GaN:RE TDEL devices [50]. The GaN:RE TDEL devices combine the full-color capability of GaN:RE phosphors with a device structure amenable to large area display fabrication. The specific advantages of the GaN:RE TDEL device structure [Fig. 15(d)] are best understood through comparison with existing ac-ELD TFEL and TDEL structures [Fig. 15(a)–(c)].

Efficient coupling of voltage and, therefore, electric field (1–2 MV/cm) to the phosphor layer in a standard all-thin-film ac-ELD [Fig. 15(a), (b)] requires dielectrics which are free of pinholes and other defects and exhibit a high dielectric constant ($\varepsilon_r \sim$ 20–30) and/or high breakdown field (4–7 MV/cm). Recent improvements in ac-ELD fabrication have led to the use of very high permittivity thick-dielectric films. There are two embodiments of these TDEL device structures. The *inverted* (I)-TDEL device [51] approach is shown in Fig. 15(c). I-TDEL is structurally superior to TFEL ac-ELDs in capacitance (device efficiency) and ease of large area fabrication due to use of a screen printed (and sintered) thick-film dielectric layer. The thick dielectric layer is unaffected by micron-sized defects
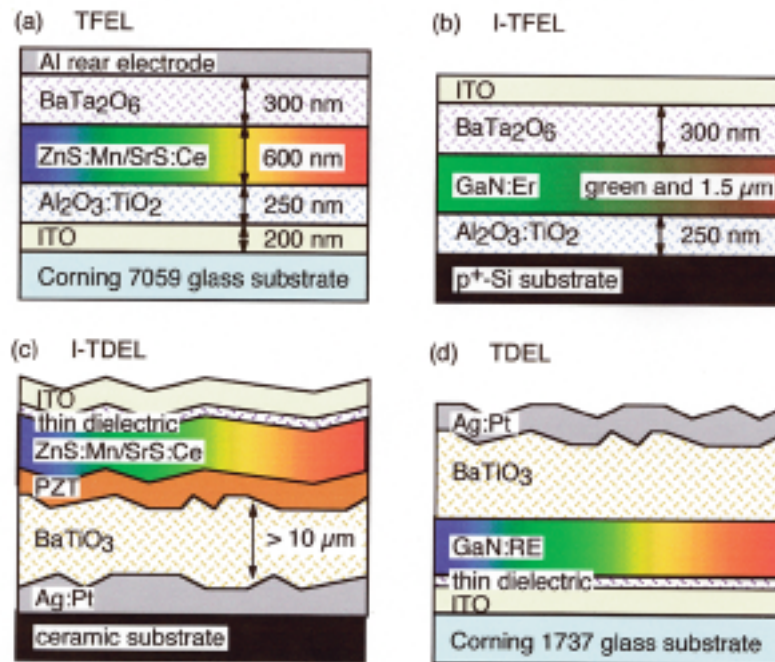
Fig. 15.   Cross-section schematic of alternative ac-ELD structures: (a) thin-film EL-TFEL; (b) inverted thin-film EL-I-TFEL; (c) inverted thick-dielectric EL-I-TDEL; (d) thick-dielectric EL-TDEL.

or contaminants, which would cause catastrophic failure of thin-film dielectrics. However, the I-TDEL approach requires formation of the opaque thick-film dielectric layer *before* the phosphor layer. This is required because the ZnS:Mn/SrS:Ce phosphor is incompatible with the byproducts produced and temperature required by the dielectric sintering cycle [52]. This, in turn, leads to the inverted designation for the device since light must be emitted away from the substrate given that the thick dielectric layer is generally opaque. Adding further difficulty, prior to phosphor deposition the thick dielectric surface must be smoothed by an additional sol-gel planarization layer. GaN:RE TDEL devices are *noninverted* and emit light through the glass substrate. As a result, these TDEL devices require no planarization layer since the phosphor layer is deposited before the thick-film dielectric is applied.

The substrate of choice for TDEL structures is presently high-temperature-stable Corning 1737 glass which is widely utilized for active matrix liquid crystal displays. The thick dielectric allows for tolerance of slight substrate surface defects. Therefore, the TDEL structures are fabricated on industrial grade 1737 glass which is ∼1/3 the cost of display grade 1737. The 1737 glass substrates are first coated with ITO for use as a transparent front electrode. GaN:RE phosphor is then deposited with (or without) surrounding thin-film dielectric layers. Following phosphor deposition, one or two layers of dielectric paste are screen printed through a wire mesh. The dielectric paste contains BaTiO$_3$ along with glass or fluxing agents which facilitate low temperature sintering of the dielectric. Following printing, the dielectric layer is dried and then sintered for ∼5–10 min at a temperature which can range between 600 °C to 800 °C. The sintered thick dielectric has a thickness in the range of 10 to 40 μm (one or more prints), a breakdown strength of ∼0.1–0.4 MV/cm, and a dielectric constant of $\varepsilon_r \sim 500$–1000.

The device is then completed by sputtering or screen printing of a rear metal electrode. Since thick-film processing is utilized for the rear dielectric, the device can tolerate up to micrometer-sized contaminants without loss of reliability. The emission from a finished GaN:RE TDEL device is uniform to dimensions less than 10 μm which exceeds display pixel requirements (∼100 μm to several millimeters).

B. Black Dielectric TDEL

Usage of light emitting devices for displays places an additional device requirement of low reflectivity of ambient light, commonly referred to as high contrast. Low reflectivity is important since reflected ambient light can make it difficult to resolve the emission from a display pixel. The effectiveness of a light emitting device to be legible in bright lighting is measured [53] as contrast ratio, which is defined as the sum of emitted and reflected luminance divided by reflected luminance. TFEL ac-ELDs achieve high contrast through minimizing reflectance from the rear metal electrode by optical interference or light absorption. Such techniques are not available for use in I-TDEL [Fig. 15(c)] and TDEL [Fig. 15(d)] devices since the thick-dielectric layer is a strong diffuse reflector and little or no light reaches the rear electrode before being reflected. In order to combine the fabrication advantages of a GaN:RE TDEL device with high contrast operation, we have developed a novel black thick-dielectric electroluminescent (B-TDEL) device structure. These B-TDEL devices exhibit superior device contrast which is easily observed by viewing the GaN:Eu TDEL and B-TDEL devices shown in Fig. 16. Both devices were operated up to 120 V$_p$ and 1 kHz. The BDEL operation clearly results in greater contrast. The black dielectric is formed by a pigmentation process which is highly effective in reducing the reflectivity from the thick-dielectric layer while allowing it to
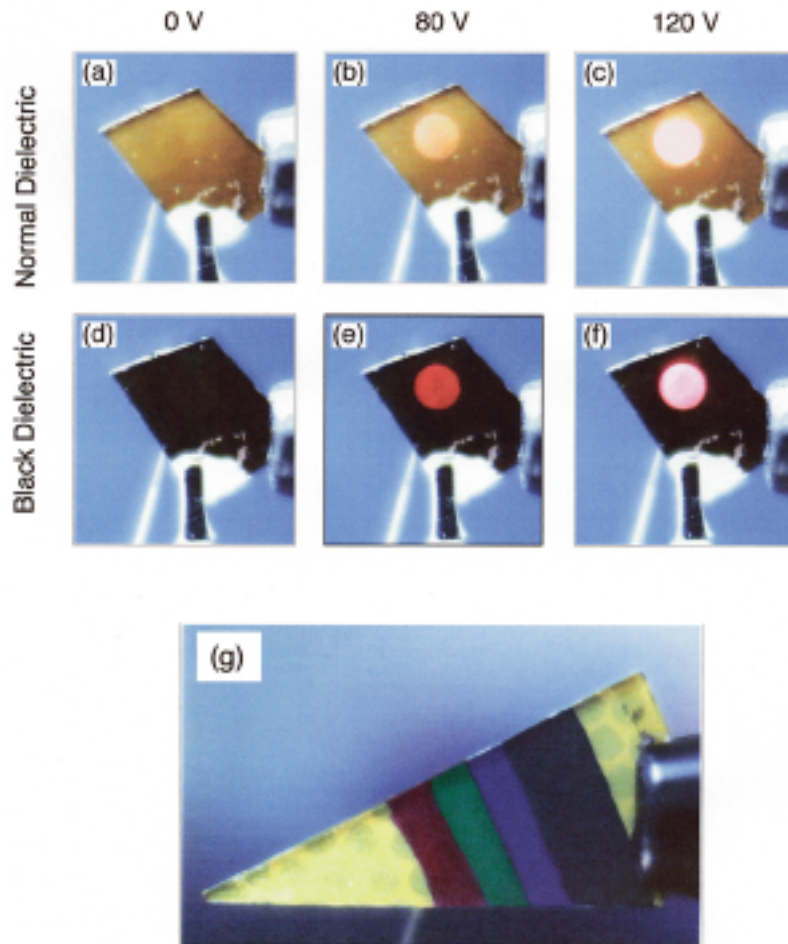
Fig. 16. Photographs showing the contrast enhancement achieved through use of a black thick-dielectric layer. The thick-dielectric GaN:Eu EL device in (a)–(c) was photographed in 140 lx white light ambient under 0, 80, and 120 V, and 1 kHz bias. The same device was then fabricated into a black thick dielectric device (d)–(f) and photographed under identical lighting and operating conditions. Shown in (g) is a range of colors that can be achieved with the impregnated thick dielectric.

retain both superior dielectric constant and breakdown voltage. The spectral reflectivity versus wavelength (specular+diffuse) from the front surface (facing 1737 glass) of a black thick dielectric and the black pigmentation medium itself are shown in Fig. 17. The unpigmented thick dielectric exhibits a diffuse reflectivity of $\sim$10%–20%. The black pigmentation medium dominates the optical characteristics of the $BaTiO_3$ thick dielectric. The measured B-TDEL diffuse reflectivity of $\sim$3% translates to a luminous reflectivity of $\sim$2.5% considering the photopic response of the human eye. Future black dielectric reflectance is expected to reach levels of 0.5%. This low level of reflectivity, in conjunction with 300 cd/m^2 TDEL device brightness, would allow for sunlight legibility (contrast ratio of 3:1 under 100 000-lx lighting conditions).

C. Prototype Fabrication

Display prototypes using GaN:RE phosphors and black B-TDEL device structures are under development at Extreme Photonix Corporation, Cincinnati, OH. A 1.5-in diagonal GaN:Eu B-TDEL display is shown in Fig. 18(a). The prototype was formed using B-TDEL fabrication techniques described in previous sections. The fixed image shown in the display was
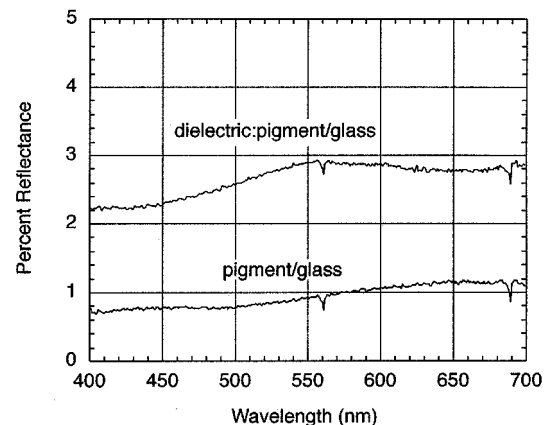

Fig. 17. Percent reflectivity as a function of wavelength for black pigment and black pigment-impregnated dielectric applied directly to a glass substrate.

formed through a combination of metal electrode sputtering and screen printing patterning. This low-cost approach, which does not require photolithography, can produce features less than 100 μm in size. The resulting resolution of the patterned image is shown in Fig. 18(b) and exceeds the resolution requirements for most flat-panel display screen formats.
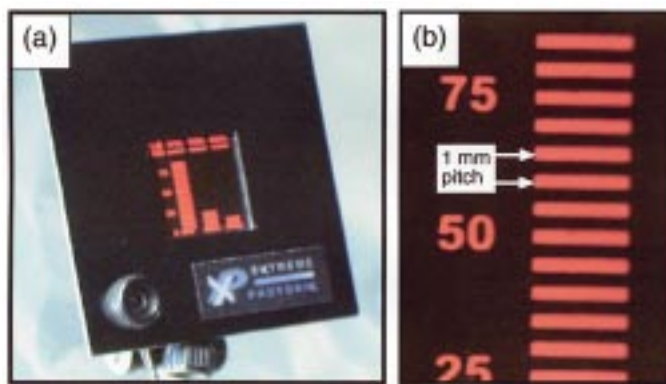
Fig. 18. GaN:Eu ac-ELD flat-panel display prototype: (a) overall dimensions—1×1 in^2; (b) pixel pitch—1 mm.

D. Multicolor Integration

As discussed in the previous sections, blue, green, and red electroluminescence have been reported from *in situ* doped GaN:RE devices. So-called mixed colors, such as turquoise or yellow, have also been obtained from GaN:RE through uniform codoping Er and Tm or Er and Eu, respectively. Two types of color integration have been pursued: vertical integration and lateral integration. In the former case, the phosphor films are placed layer upon layer, while in the latter case, the pixels are arranged side by side. The advantage of vertical integration is that the structure is compact. However, the disadvantage is that it prevents optimum operation of each color pixel. A two-color integrated ELD with stacked layers of GaN:Eu and GaN:Er has been reported [5] to emit green light under positive bias and red light under negative bias. The advantage of lateral integration is that it enables growth of each film under optimized conditions for the emission of each color [6], [54]; and that pixels can be biased at the optimum condition for each color. Yamauchi *et al.* [55] reported a two-color (red and green) TFEL device fabricated laterally by a combination of wet etching and liftoff. Since then many groups have studied and improved multicolor TFEL integration, mostly on II–VI hosts.

We have investigated two patterning techniques to obtain lateral multicolor integration: the use of liftoff techniques with either organic [56] or inorganic [57] sacrificial layers and the use of shadow masks [56] during growth of GaN:RE films.

1) Integrated Color Device Fabrication: The liftoff layer (LoL) technique when used in conjunction with an organic material (photoresist—PR) restricts the GaN:RE growth to temperatures below 100 °C. While these as-deposited films result [56] in rather weak EL emission, a post-deposition high-temperature anneal has been shown [24] to increase the emission intensity dramatically. We have also investigated the use of inorganic LoLs, specifically spin-on-glass (SOG). SOG is an attractive choice for this process for several reasons: it contains mainly SiO$_2$ and little or no organics; it can be exposed to high growth temperatures; and it can be etched off in a few seconds in an HF solution. The shadow mask deposition allows for higher GaN:RE temperature deposition than the photoresist LoL, but not as high as the SOG LoL, because of deformation in the Al foils used as masks. Use of refractory metal (W, Ta) foils as shadow masks will allow for much higher temperature
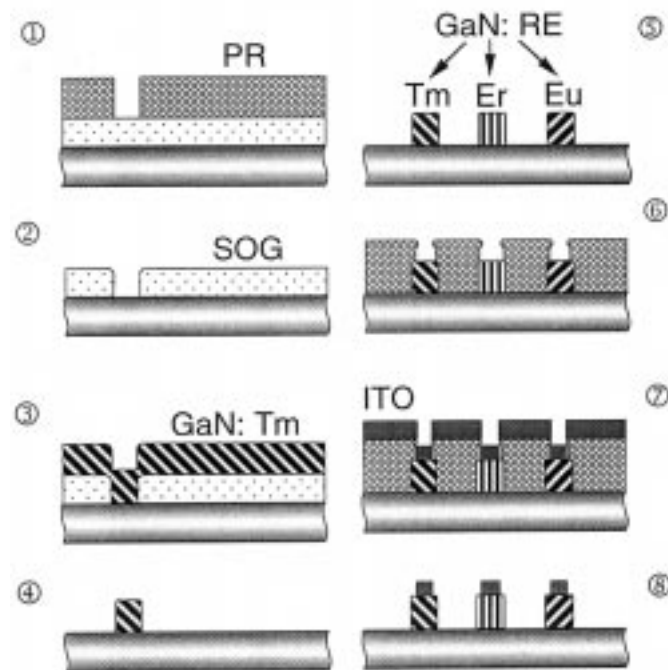

Fig. 19. Fabrication procedure for multicolor integration using the SOG lift-off approach.

deposition. In general, shadow mask techniques cannot provide the sharp features of the LoL technique because shadow masks are generally much thicker than an LoL and because they cannot provide the same level of intimate surface contact as a LoL.

The main fabrication steps for multicolor lateral integration with the SOG LoL are illustrated schematically in Fig. 19. The liftoff method consists of the following fabrication steps:

1) spin SOG on Si wafer twice, then coat PR and expose the PR pattern;
2) etch SOG with 0.1% diluted HF to form the SOG window for GaN:RE growth;
3) outgas SOG, grow GaN:Tm;
4) lift off the SOG with HF revealing the GaN:Tm pattern;
5) repeat procedures from 1) to 4) twice, but grow GaN:Er or GaN:Eu layers;
6) produce PR patterns for ITO electrodes on GaN:RE pixels;
7) sputter ITO thin films;
8) lift off PR and anneal in an N$_2$ ambient in order to increase the conductivity of the ITO electrode.

2) Integrated Color Device Characteristics: Fig. 20 shows the three-color emission from the laterally integrated GaN:RE dc-ELDs using SOG LoL. The applied voltage on the blue and green pixels is 40 V and that on the red pixel is 30 V. The dimension of the GaN:RE thin-film pattern is 0.3 mm wide and 0.8 mm long. The size of the ITO electrodes is 0.2 mm wide and 0.7 mm long, and the ELDs are separated from each other by 0.3 mm. At these dimensions, the edge of the GaN:RE region obtained by SOG LoL patterning is quite sharp.

All of the color emissions are bright enough to be easily viewed with the naked eye under normal ambient lighting conditions. The emission brightness of each color pixel is shown as
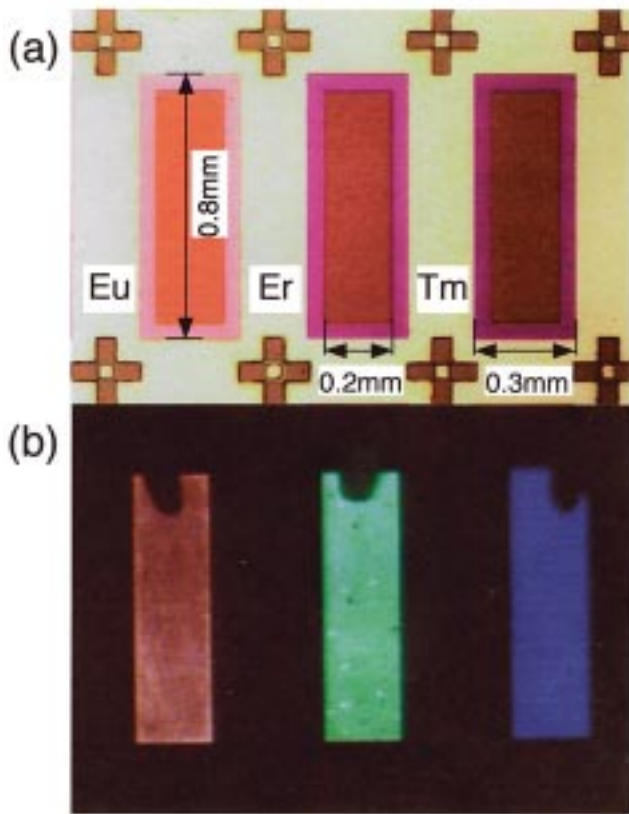
Fig. 20. Laterally-integrated, full-color GaN:RE dc-ELDs: (a) reflected light photograph of individual GaN:RE elements—0.3×0.8 mm^2; ITO electrode—0.2×0.7 mm^2; (b) simultaneous red (GaN:Eu), green (GaN:Er), and blue (GaN:Tm) emission from devices under dc bias.

Fig. 21. EL brightness from individual color pixels in a full-color GaN:RE dc ELD array as a function of applied voltage.

a function of voltage in Fig. 21. A turn-on voltage for emission of 25–30 V is observed. Above this threshold, the emission of all three pixels increases more or less linearly with voltage, with green emission from the GaN:Er pixel being the strongest.

In this section, we have described lateral multicolor integration of GaN:RE dc-ELDs by both organic and inorganic liftoff and by shadow mask techniques. We have demonstrated three-color integration using liftoff with SOG sacrificial layers, which appears to be the most practical integration approach. This is an important milestone in the progression toward the fabrication of full-color GaN:RE flat-panel displays.

V. APPLICATION TO 1.5-μm OPTICAL TELECOMMUNICATION

The applicability of GaN:RE materials to infrared ELDs has been shown in the previous sections. GaN:Er is of special interest since it has been shown to be relatively immune to the thermal quenching [39] seen in other Er-doped semiconductors and has the ability to incorporate significant concentration [27] of RE ions without precipitation and without quenching the photoluminescence or electroluminescence intensity. These properties, in conjunction with the fact that GaN is a semiconductor and can provide charge carrier excitation of the Er ions (unlike insulators such as SiO$_2$:Er), meet the key requirements for an electrically pumped waveguide amplifier.

To determine the potential of next generation GaN integrated optic devices and systems, we have characterized the operation of
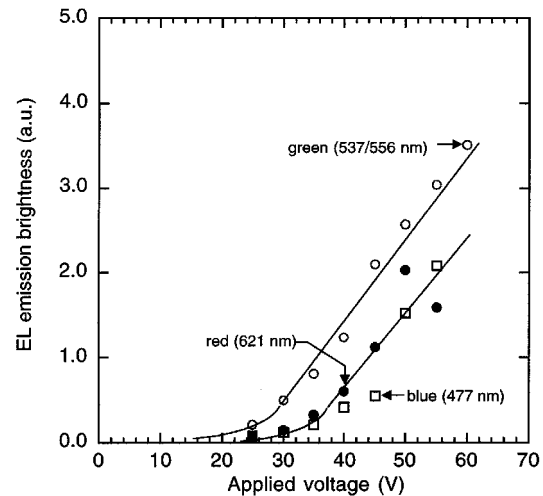
GaN optical waveguides in the infrared regime. While there have been several reports of GaN waveguide operation in the UV and visible regimes [58], this is believed to be the first report of quantitative loss measurements taken in the infrared regime for GaN channel waveguides. This will be of great importance in determining tolerances of future GaN integrated optic systems operating in the infrared as well as providing a baseline for GaN:RE optical waveguides that can serve as an amplifying medium.

Paramount to the development of waveguides in any material is the ability to achieve etched surfaces with morphology comparable to the smooth unetched surface. Unfortunately, there is no simple effective wet etchant for GaN. To overcome these difficulties, we have initiated the development of an inductively coupled plasma (ICP) etch process specifically for the fabrication of GaN and GaN:Er waveguides. ICP etching of GaN and its alloys has been reported [59] to provide smooth surfaces under properly designed etch conditions.

A. GaN Channel Waveguide Fabrication by ICP

Two different GaN materials were studied. The first material utilized was commercially available GaN on Al$_2$O$_3$ obtained from TDI, Inc. This material consisted of an undoped 1.6-μm GaN layer grown on a double-side-polished Al$_2$O$_3$ substrate by metallorganic chemical vapor deposition (MOVCD). The second material was our own GaN:Er grown by MBE on Al$_2$O$_3$ substrates at 600 °C. The Er concentration was estimated to be 0.5–1 at.%. The crystalline, undoped commercial GaN was included in the etching experiments in order to provide "baseline" results for an extensive investigation into the properties of GaN and GaN:Er waveguides. GaN:RE material has been optimized for light emission in other photonic applications, but has not yet been fully optimized in terms of optical transmission and scattering properties. The GaN:Er in this investigation was grown under conditions for smooth morphology and optical transparency.

The materials were etched using a PlasmaTherm 790 plasma reactor in ICP mode. The only etch mask used was a 1.8-μm-thick layer of Shipley 1818 positive photoresist. The pattern consisted of parallel 5-μm-wide straight lines. These lines enabled the etching of the ridge waveguide structure
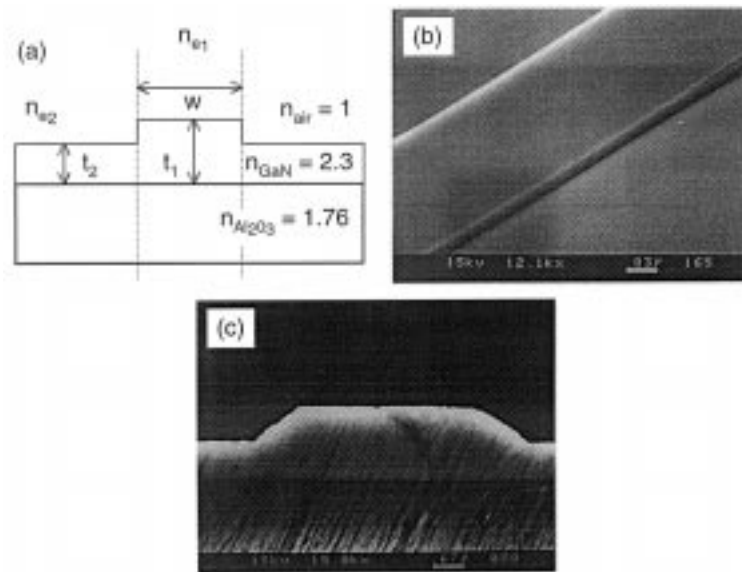
Fig. 22.   GaN channel waveguide: (a) cross-section schematic; (b) SEM photograph of waveguide—top view; (c) SEM photograph of waveguide—cross section.

shown in the schematic in Fig. 22(a). A Cl_2/Ar-based plasma etch chemistry was selected and optimized for commercial GaN material by varying the ICP power from 300 to 700 W and the RF power from 80 to 120 W. An Ar flow of 5 sccm, Cl_2 flow of 15 sccm, and chamber pressure of 5 mtorr were kept constant during all experiments. We have observed that increasing the ICP power produces higher etch rates, while the RF power is the most critical etching parameter in terms of local morphology. A moderate ICP power of 500 W was chosen and nearly flawless etching resulted from an RF power of 100 W. This is illustrated in the scanning electron microscope (SEM) photograph of a GaN waveguide shown in Fig. 22(b). The polished cross section of a waveguide with a ridge height of 900 nm is shown in the SEM photograph of Fig. 22(c). It has been shown [60] that sloping sidewalls produce very little mode perturbation and may select the base width of the rib when using the effective index technigue.

Fig. 23 shows the etch rates obtained for the undoped and doped GaN films etched under the same conditions of 500 W ICP power and 100 W RF power. The etch rate of the undoped GaN is ~400 nm/min, while Er-doped GaN film exhibits a much slower rate of ~100 nm/min. This is somewhat surprising since the undoped material is crystalline and the GaN:Er film has a polycrystalline structure at best. Usually, a reduction in crystallinity is accompanied by an increase in etch rate due to the many weaker and/or broken bonds. A possible explanation lies in the difference in electrical conductivity of the two materials, with the Er-doped GaN film actually being much more resistive than the "undoped" film. Surface charge carriers are known [61] to play a critical role in the etching process and their absence could certainly reduce the etch rate.

B. GaN Channel Waveguide Design and Characterization

GaN optical channel waveguides were designed for use with the commercial material using the well-known effective index method [62]. GaN refractive index values of ~2.35 and ~2.25 at 632.8 nm and 1.5 μm were previously reported [63]. We have
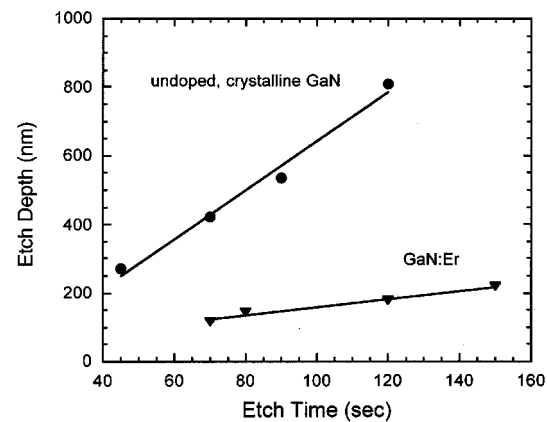

Fig. 23.   GaN waveguide fabrication by inductively coupled plasma etching: etch depth versus time.

measured a GaN refractive index of 2.352 at 632.8 nm using the prism coupling method. The refractive index of sapphire [64] changes from ~1.77 to ~1.75 in the same wavelength range of 632.8 nm to 1.5 μm. A ridge width of 5 μm was fixed by the dimensions of the lithographic mask mentioned above. Using the fixed values of the width (w) and film thickness (t_1), n_e was calculated using the effective indices for the etched region (n_{e1}) and the unetched region (n_{e2}). An etch depth of ~0.3 μm was chosen since the resulting structure would have an appropriate effective index difference (n_e) and support only a few modes, limiting the effect of higher order lossy modes.

Optical characterization was performed using the out-scattering technique. This technique [65] assumes that the scattering centers are uniformly distributed and that the intensity of the scattered light in the transverse direction at a given point is proportional to the amount of light propagating in the waveguide at that point. Out-scattered light intensity was measured at 50 μm intervals. The waveguide facets were polished in order to reduce roughness that would scatter excess light. Channel loss measured at one visible (633 nm) and two infrared (1307 and 1500 nm) wavelengths is shown in Fig. 24. The channel loss decreases from a value of 5.4 dB/cm at 633 nm to a low of 4.1 dB/cm at
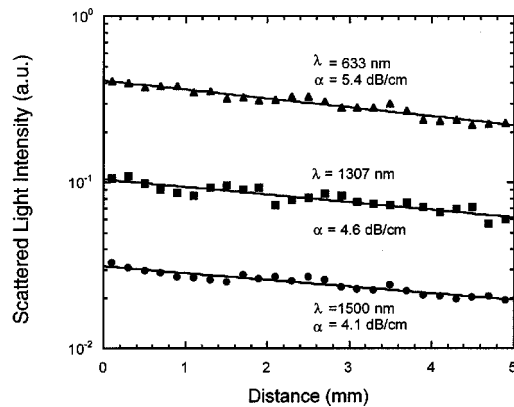
Fig. 24. GaN channel waveguide loss at visible (633 nm) and IR wavelengths (1.3 and 1.5 μm).

1550 nm. The GaN loss values we have achieved in a short period of time are only within a factor of 2 of the values reported for GaAs waveguides [66], [67] which have been under development for a much longer period of time. This clearly indicates the promise of GaN:Er-based technology for 1.5-μm optical communication applications.

VI. CONCLUSION

We have presented a review of the materials and device aspects of RE-doped GaN. GaN films doped with REs such as Eu, Er, Tm, emit red, green, and blue light, respectively. These are relatively pure colors, produced by inner shell RE transitions. The GaN provides a very robust semiconductor host which can accept a large, optically active RE concentration and can withstand the high fields needed to provide hot carriers for impact excitation of the RE ions in ELDs. GaN:RE growth mechanisms were reviewed and conclusions obtained on optimization of the GaN layers for RE emission. The fabrication processes and electrical models for both dc- and ac-biased ELDs were reviewed. Multicolor lateral integration was achieved using several techniques. Devices based on GaN:RE and designed specifically for flat-panel displays were presented. A high contrast FPD device using a black thick dielectric was described. A second application area of GaN:RE technology is infrared optical telecommunications at 1.3 and 1.5 μm. The fabrication and characteristics of GaN:Er channel waveguides for 1.5-μm operation were also reviewed. The versatility and robust nature of RE-doped GaN technology holds great promise for optoelectronic and photonic applications.

ACKNOWLEDGMENT

REFERENCES

[1] G. Blasse and B. C. Grabmaier, *Luminescent Materials*. Berlin, Germany: Springer-Verlag, 1994.
[2] P. N. Favennec, H. L'Haridon, M. Salvi, D. Moutonnet, and Y. LeGuillou, "Luminescence of erbium implanted in various semiconductors: IV, III-V and II-VI materials," *Electron. Lett.*, vol. 25, pp. 718–719, 1989.
[3] A. J. Steckl and J. M. Zavada, "Optoelectronic properties and applications of rare-earth-doped GaN," *Mater. Res. Bull.*, vol. 24, pp. 33–38, 1999.
[4] A. J. Steckl, J. Heikenfeld, M. J. Garter, R. H. Birkhahn, and D. S. Lee, "Rare earth doped gallium nitride—Light emission from ultraviolet to infrared," *Compound Semicond.*, vol. 6, pp. 48–52, 2000.
[5] A. J. Steckl, J. Heikenfeld, D. S. Lee, and M. J. Garter, "Multiple color capability from rare earth doped gallium nitride," *Mater. Sci. Eng,. B*, vol. 81/1–81/3, pp. 97–101, 2001.
[6] *Selected reviews of electroluminescent materials and devices can be found in the following.* (a) Y. A. Ono, *Electroluminescent Displays*, vol. 1 in *Series on Information Displays*, H. L. Ong, ed., World Scientific, Singapore, 1995. (b) J. F. Wager and P. D. Keir, "Electrical characterization of thin film electroluminescent devices," *Annu. Rev. Mater. Sci.*, vol. 27, pp. 223–248, 1997. (c) P. D. Rack and P. H. Holloway, "The structure, device physics, and material properties of thin film electroluminescent displays," *Mater. Sci. Eng. R*, vol. 21, no. 4, pp. 171–219, 1998. (d) G. Mueller, ed., *Electroluminescence II*, Academic, San Diego, CA, 2000.
[7] H. Morkoc, *Nitride Semiconductors and Devices*. Berlin, Germany: Springer-Verlag, 1999.
[8] R. G. Wilson, R. N. Schwartz, C. R. Abernathy, S. J. Pearton, N. Newman, M. Rubin, T. Fu, and J. M. Zavada, "1.54 μm photoluminescence from erbium and oxygen co-implanted GaN," *Appl. Phys. Lett.*, vol. 65, pp. 992–994, 1994.
[9] A. J. Steckl and R. H. Birkhahn, "Visible emission from Er-doped GaN grown by solid source molecular beam epitaxy," *Appl. Phys. Lett.*, vol. 73, pp. 1700–1702, 1998.
[10] A. J. Steckl, M. J. Garter, R. H. Birkhahn, and J. Scofield, "Green electroluminescence from Er-doped GaN Schottky barrier diodes," *Appl. Phys. Lett.*, vol. 73, pp. 2450–2452, 1998.
[11] M. J. Garter, J. D. Scofield, R. H. Birkhahn, and A. J. Steckl, "Visible and infrared emission from ITO/GaN:Er/Si Schottky diodes," *Appl. Phys. Lett.*, vol. 74, pp. 182–184, 1999.
[12] R. H. Birkhahn, M. J. Garter, and A. J. Steckl, "Red light emission by photoluminescence and electroluminescence from Pr-doped GaN on Si substrates," *Appl. Phys. Lett.*, vol. 74, pp. 2161–2163, 1999.
[13] J. Heikenfeld, M. J. Garter, D. S. Lee, R. H. Birkhahn, and A. J. Steckl, "Red light emission by photoluminescence and electroluminescence from Eu-doped GaN," *Appl. Phys. Lett.*, vol. 75, pp. 1189–1191, 1999.
[14] A. J. Steckl, M. J. Garter, D. S. Lee, J. Heikenfeld, and R. H. Birkhahn, "Blue electroluminescence from Tm-doped GaN light emitting devices," *Appl. Phys. Lett.*, vol. 75, pp. 2184–2186, 1999.
[15] C. H. Qiu, M. W. Leksono, J. I. Pankove, J. T. Torvik, R. J. Feurstein, and F. Namavar, "Cathodoluminescence study of erbium and oxygen co-implanted GaN thin films on sapphire substrates," *Appl. Phys. Lett.*, vol. 66, pp. 562–564, 1995.
[16] S. Kim, S. J. Rhee, D. A. Ternbull, E. F. Reuter, X. Li, J. J. Coleman, and S. G. Bishop, "Observation of multiple Er^{3+} sites in Er-implanted GaN by site-selective photoluminescence excitation spectroscopy," *Appl. Phys. Lett.*, vol. 71, pp. 231–233, 1997.
[17] J. T. Torvik, C. H. Qiu, R. J. Feurstein, J. I. Pankove, and F. Namavar, "Photo-, cathodo-, and electroluminescence from erbium and oxygen co-implanted GaN," *J. Appl. Phys.*, vol. 81, pp. 6343–6350, 1997.
[18] D. M. Hansen, R. Zhang, N. R. Perkin, S. Safvi, L. Zhang, K. L. Bray, and T. F. Keuch, "Photoluminescence of erbium-implanted GaN and in-situ doped GaN:Er," *Appl. Phys. Lett.*, vol. 72, pp. 1244–1246, 1998.
[19] H. J. Lozykowski, W. M. Jadwisienczak, and I. Brown, "Photoluminescence and cathodoluminescence of GaN doped with Pr," *J. Appl. Phys.*, vol. 88, pp. 210–222, 2000.
[20] J. D. Mackenzie, C. R. Abernathy, S. J. Pearton, U. Hommerich, X. Wu, R. N. Schwartz, R. G. Wilson, and J. M. Zavada, "Er doping of III-nitrides during growth by metalorganic molecular beam epitaxy," *J. Cryst. Growth*, vol. 175/176, pp. 84–88, 1997.
[21] R. H. Birkhahn, R. A. Hudgins, D. S. Lee, A. J. Steckl, R. J. Molnar, and J. M. Zavada, "Growth and morphology of Er-doped GaN on sapphire and HVPE substrates," *J. Vac. Sci. Technol. B*, vol. 17, pp. 1195–1199, 1999.
[22] K. Lorenz, R. Vianden, R. H. Birkhahn, A. J. Steckl, M. F. da Silva, J. C. Soares, and E. Alves, "RBS/Channeling study of Er-doped GaN films grown by MBE on (111) Si substrates," *Nucl. Instr. Meth. B*, vol. 161/163, pp. 946–951, 2000.
[23] P. H. Citrin, P. A. Northrup, R. H. Birkhahn, and A. J. Steckl, "Local structure and bonding of Er in GaN: A contrast with Er in Si," *Appl. Phys. Lett.*, vol. 76, pp. 2865–2867, 2000.
[24] D. S. Lee and A. J. Steckl, "Room-temperature-grown rare-earth-doped GaN luminescent thin films," *Appl. Phys. Lett.*, vol. 79, pp. 1962–1964, 2001.

[25] H. Sasakura, H. Kobayashi, S. Tanaka, J. Mita, T. Tanaka, and H. Nakayama, "The dependences of electroluminescent characteristics of ZnS:Mn thin films upon their device parameters," *J. Appl. Phys.*, vol. 52, pp. 6901–6906, 1981.

[26] D. S. Lee, J. Heikenfeld, R. H. Birkhahn, M. J. Garter, and A. J. Steckl, "Voltage-controlled yellow or orange emission from GaN co-doped with Er and Eu," *Appl. Phys. Lett.*, vol. 76, pp. 1525–1527, 2000.

[27] D. S. Lee, J. Heikenfeld, A. J. Steckl, U. Hommerich, J. T. Seo, A. Braud, and J. M. Zavada, "Optimum Er concentration for *in situ* doped GaN visible and infrared luminescence," *Appl. Phys. Lett.*, vol. 79, pp. 740–742, 2001.

[28] D. J. Eaglesham, J. Michel, E. A. Fitzgerald, D. C. Jacobson, J. M. Poate, J. L. Benton, A. Polman, Y.-H. Xie, and L. C. Kimerling, "Microstructure of erbium-implanted Si," *Appl. Phys. Lett.*, vol. 58, pp. 2797–2799, 1991.

[29] A. Taguchi, M. Kawashima, K. Takahei, and Y. Horikoshi, "Er luminescence centers in GaAs grown by migration-enhanced epitaxy," *Appl. Phys. Lett.*, vol. 63, p. 1074, 1993.

[30] E. Alves, R. C. da Silva, M. F. da Silva, and J. C. Soares, "Solubility and damage annealing of Er implanted single crystalline a-Al_2O_3," *Nucl. Instr. Meth. B*, vol. 139, pp. 313–317, 1998.

[31] J. D. MacKenzie, C. R. Abernathy, S. J. Pearton, U. Hommerich, X. Wu, R. N. Schwartz, R. G. Wilson, and J. M. Zavada, "Er doping of AlN during growth by metal organic molecular beam epitaxy," *Appl. Phys. Lett.*, vol. 69, pp. 2083–2085, 1996.

[32] T. Kano, *Phosphor Handbook.* Boca Raton, FL: CRC, 1999, vol. 185.

[33] D. S. Lee, J. Heikenfeld, and A. J. Steckl, "Growth-temperature dependence of Er-doped GaN luminescent thin films," *Appl. Phys. Lett.*, vol. 80, pp. 344–346, 2002.

[34] E. Calleja, M. A. Sanchez-Garcia, F. J. Sanchez, F. Calle, F. B. Naranjo, E. Munoz, U. Jahn, and K. Ploog, "Luminescence properties and defects in GaN nanocolumns grown by molecular beam epitaxy," *Phys. Rev. B*, vol. 62, pp. 16 826–16 834, 2000.

[35] D. S. Lee and A. J. Steckl, "Ga flux dependence of Er-doped GaN luminescent thin films," *Appl. Phys. Lett.*, vol. 80, pp. 728–730, 2002.

[36] R. Raghunathan and B. J. Baliga, "Role of defects in producing negative temperature dependence of breakdown in SiC," *Appl. Phys. Lett.*, vol. 72, pp. 3196–3198, 1998.

[37] J. K. Sheu, Y. K. Su, G. C. Chi, M. J. Jou, and C. M. Chang, "Effects of annealing on the indium tin oxide Schottky contacts of *n*-GaN," *Appl. Phys. Lett.*, vol. 72, pp. 3317–3319, 1998.

[38] T. Margalith, O. Buchinsky, D. A. Cohen, A. C. Abare, M. Hansen, S. P. DenBaars, and L. A. Coldren, "Indium tin oxide contacts to gallium nitride optoelectronic devices," *Appl. Phys. Lett.*, vol. 74, pp. 3930–3932, 1999.

[39] M. J. Garter and A. J. Steckl, "Temperature behavior of visible and infrared electroluminescent devices fabricated on Er-doped GaN," *IEEE Trans. Electron Devices*, vol. 49, pp. 48–54, Jan. 2002.

[40] A. M. Emel'yanov, N. A. Sobolev, and A. N. Yakimenko, "Anomalous temperature dependence of erbium-related electroluminescence in reverse biased *p-n* junctions," *Appl. Phys. Lett.*, vol. 72, pp. 1223–1225, 1998.

[41] C. Du, W. Ni, K. B. Joelsson, and G. V. Hansson, "Room temperature 1.54 μm light emission of erbium doped Si Schottky diodes prepared by molecular beam epitaxy," *Appl. Phys. Lett.*, vol. 71, pp. 1023–1025, 1997.

[42] S. J. Chang and K. Takahei, "Studies of GaAs:Er impact excited electroluminescent devices," *Appl. Phys. Lett.*, vol. 65, pp. 433–435, 1994.

[43] G. M. Ford and B. W. Wessels, "Electroluminescence from forward biased Er-doped GaP *p-n* junctions at room temperature," *Appl. Phys. Lett.*, vol. 68, pp. 1126–1128, 1996.

[44] L. Ke, S. J. Chua, K. Zhang, and N. Yakovlev, "Degradation and failure of organic light-emitting devices," *Appl. Phys. Lett.*, vol. 80, pp. 2195–2197, 2002.

[45] M. J. Russ and D. I. Kennedy, "The effects of double insulating layers on the electroluminescence of evaporated ZnS:Mn films," *J. Electrochem. Soc.*, vol. 114, pp. 1066–1072, 1967.

[46] J. Heikenfeld and A. J. Steckl, "Alternating current thin-film electroluminescence of GaN:Er," *Appl. Phys. Lett.*, vol. 77, pp. 3520–3522, 2000.

[47] R. Mueller-Mach and G. Mueller, "Thin film electroluminescence," in *Electroluminescence II.* San Diego, CA: Academic, 2000, ch. 2, p. 49.

[48] U. Hommerich, J. T. Seo, C. R. Abernathy, A. J. Steckl, and J. M. Zavada, "Spectroscopic studies of the visible and infrared luminescence from Er-doped GaN," *Mater. Sci. Eng., B*, vol. 81/1–81/3, pp. 116–120, 2001.

[49] X. Wu, "Asia display," in *Proc. Int. Display Workshop*, 2001, pp. 1055–1058.

[50] J. Heikenfeld and A. J. Steckl, "Electroluminescent devices on glass using a high temperature stable GaN-based phosphor and thick film dielectric," *IEEE Trans. Electron Devices*, vol. 49, pp. 557–563, Apr. 2002.

[51] P. Bailey, D. Carkner, and X. Wu, "Trailing edge light emission from ZnS:Mn and ZnS:Tb in a thick dielectric electroluminescent display," *J. Appl. Phys.*, vol. 81, pp. 931–936, 1997.

[52] I. Burn and L. Drozdyk, "Reliability of thick film capacitors," in *Proc. Int. Soc. Hybrid Microelectronics*, 1992, pp. 439–444.

[53] M. Ylilammi, "Optical properties of ACTFEL displays," *J. Soc. Inf. Display*, vol. 3/2, pp. 59–66, 1995.

[54] G. Harkonen, M. Leppanen, E. Soininen, R. Tornqvist, and J. Viljanen, "Multicolor thin film electroluminescent displays: A new application of rare earth metals," *J. Alloys Comp.*, vol. 225, pp. 552–554, 1995.

[55] N. Yamauchi, H. Kozawaguchi, O. Koure, and B. Tsujiyama, "A multicolor thin-film electroluminescent device with patterned phosphors," in *Proc. Dig. 1987 SID Int. Symp.*, 1987, pp. 230–233.

[56] D. S. Lee and A. J. Steckl, "Lateral color integration on rare-earth-doped GaN electroluminescent thin films," *Appl. Phys. Lett.*, vol. 80, pp. 1888–1890, 2002.

[57] Y. Q. Wang and A. J. Steckl, "Three color integration on rare-earth-doped GaN electroluminescent thin films", to be published.

[58] T. Tanaka, K. Uchida, A. Watanabe, and S. Minagawa, "Observation of stimulated emission, line narrowing, and red shift of emission peak from optically-pumped rectangular cross sectional GaN optical waveguides fabricated by selective growth," *Electron. Lett.*, vol. 32, pp. 34–36, 1996.

[59] H. Cho, C. B. Vartuli, C. R. Abernathy, S. M. Donovan, S. J. Pearton, R. J. Shul, and J. Han, "Cl_2-based dry etching of the AlGaInN system in inductively coupled plasmas," *Solid State Electron.*, vol. 42, pp. 2277–2281, 1998.

[60] N. Dogli and C. G. Fonstad, "Analysis of rib waveguides with sloped rib sides," *Appl. Phys. Lett.*, vol. 46, pp. 529–531, 1985.

[61] D. L. Flamm, "Introduction to plasma chemistry," in *Plasma Etching*, D. M. Manos and D. L. Flamm, Eds. New York: Academic, 1989, ch. 2.

[62] J. T. Boyd, "Photonic indegrated circuits," in *Photonic Devices and Systems*. New York: Marcel Dekker, 1994, ch. 9.

[63] G. Yu, G. Wang, H. Ishikawa, M. Umeno, T. Soga, T. Egawa, J. Watanabe, and T. Jimbo, "Optical properties of wurtzite structure GaN on sapphire around fundamental absorption edge (0.78–4.77 eV) by spectroscopic ellipsometry and the optical transmission method," *Appl. Phys. Lett.*, vol. 70, pp. 3209–3211, 1997.

[64] "Industrial Data Sheet," Meller Optics, Providence, RI.

[65] M. Kumar, "Optical Channel Waveguide Formation by Focused Ion Beam Induced Selective Mixing and Wet Chemical Etching," Ph.D. dissertation, Univ. of Cincinnati, Cincinnati, OH, 1996.

[66] D. A. Andrews, E. G. Scott, A. J. N. Houghton, P. M. Rodgers, and G. J. Davies, "The growth of GaAlAs/GaAs guided wave devices by molecular beam epitaxy," *J. Vac. Sci. Technol., B*, vol. 3, pp. 813–815, 1985.

[67] R. J. Shul, C. T. Sullivan, M. B. Snipes, G. B. McClellan, M. Hafich, C. T. Fuller, C. Constantine, W. Less, and S. J. Pearton, "Attenuation losses in electron cyclotron resonance plasma etched AlGaAs waveguides," *Solid State Electron.*, vol. 38, pp. 2047–2049, 1995.
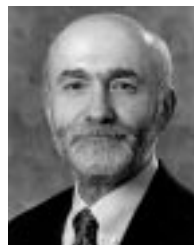
Andrew J. Steckl (S'70–M'73–SM'79–F'99) received the B.S.E. degree in electrical engineering from Princeton University, Princeton, NJ, and the M.Sc. and Ph.D. degrees from the University of Rochester, Rochester, NY, in 1968, 1970, and 1973, respectively.

In 1972, he joined the Honeywell Radiation Center, Lexington, MA, as a Senior Reserch Engineer, where he worked on new concepts and devices in the area of infrared detection. In 1973, he joined the Technical Staff of the Electronics Research Division, Rockwell International, Anaheim, CA. At Rockwell, he was primarily involved in research on charge coupled devices. In 1976, he joined the Electrical, Computer, and Systems Engineering Department, Rensselaer Polytechnic Institute, Troy, NY, where he developed a research program in microfabrication of Si devices. In 1981, he founded the Center for Integrated Electronics, a multidisciplinary academic center focused on VLSI research and teaching, and served as its Director until 1986. In 1988, he joined the Electrical and Computer Engineering Department, University of Cincinnati, OH, as Ohio Eminent Scholar and Gieringer Professor of Solid State Microelectronics. At the University of Cincinnati, he has been with the Nanoelectronics Laboratory, where his research interests include semiconductor materials and devices for photonics, SiC and GaN thin-film growth by CVD and MBE, focused ion beam fabrication of photonic components and circuits, rare-earth-doped luminescent devices for flat-panel displays, and communications. He has authored over 290 published articles and over 300 conference and seminar presentations.

Jason C. Heikenfeld (S'99) received the B.S. and Ph.D. degrees from the University of Cincinnati, OH in 1998 and 2001, respectively. His major was in electrical engineering with minors in both photonics and physics. His doctoral study was supported by the University of Cincinnati Distinguished Graduate Assistantship and concentrated on novel inorganic electroluminescent display devices based on RE-doped GaN.

He is currently a Research Scientist with Extreme Photonix Corporation, Cincinnati, OH. His main duties include leading the development of ELDs for flat-panel displays. He has authored and coauthored more than 20 publications in refereed journals, conference proceedings, and a book chapter. He is an inventor on three pendings U.S. patents.

Dr. Heikenfeld is a member of the Society for Information Display, Materials Research Society, and the American Society for Engineering Education.

Dong-Seon Lee (S'00) received the B.S. and M.S. degree in physics from Seoul National University, Seoul, Korea, and the Ph.D. degree from the University of Cincinnati, OH, in 1987, 1989, and 2002, respectively. His doctoral study at the Nanoelectronics Laboratory focused on the growth, fabrication, characterization, and optimization of rare-earth-doped GaN for the purpose of ELDs and studying luminescent mechanisms.

In 1991, he joined Samsung Electronics Company, Ltd., Kiheung, South Korea, as a Photolithography Engineer, where he worked on the development of the 64, 256 Mbit, and 1 Gbit DRAM. In 1997, he joined the Nanoelectronics Laboratory at the University of Cincinnati, where he is now a Research Associate with the Nanoelectronics Laboratory. His research interests include the further improvement and optimization of rare-earth-doped GaN growth, fabrication, and devices. He has authored and coauthored more than 20 publications in referreed journals and conference proceedings.

Michael J. Garter received the B.S. degree in electrical engineering and the Ph.D. degree from the University of Cincinnati, Cincinnati, OH in 1996 and 2001, respectively. His undergraduate research led to the fabrication of silicon micro-mirrors using MEMS techniques.

In 1996, he joined the Nanoelectronics Laboratory, the University of Cincinnati. During the first two years at the NanoLab, he focused on plasma etching of SiC and GaN. His focus then shifted to the MBE growth, fabrication, and testing of erbium-doped GaN ELDs. During his graduate work, he gave several formal presentations, including a paper at the Device Research Conference in June, 1999. His graduate research has also resulted in the publication of over 10 papers and a U.S. patent on RE-doped GaN electroluminescence. He is currently with CMC Electronics Cincinnati, Mason, OH, where he works on the fabrication and optimization of infrared light detection products.

Christopher C. Baker (S'00) received the B.S. degree in physics in 1998 from Miami University, Oxford, OH. His undergraduate research was in the field of giant magnetoresistance for which he received funding through Miami University's Undergraduate Summer Scholar program. He is currently working toward the Ph.D. degree in electrical engineering at the University of Cincinnati, Cincinnati, OH, where he is focused on active and passive integrated optic components.

In 2001 he joined the Nanoelectronics Laboratory, University of Cincinnati, as a Research Associate to develop novel GaN photonic devices.

Yongqiang Wang received the B.S. degree in physics and M.S. degree from Suzhou University, Suzhou, China, and the Ph.D. degree from the Institute of Physics, Chinese Academy of Science, Beijing, China, in 1991, 1994, and 1997, respectively. His doctoral research led to the fabrication of GaAs/AlGaAs quantum wires using cleaved-edge-overgrowth technique by molecular beam epitaxy.

In 1997, he joined Department of Physics, Peking University, Beijing, China, as a postdoctoral student, where he worked on electroluminescence of nanometer Si structure. In 1999, he joined Japan Fine Ceramics Center, Nagoya, Japan, as an STA fellow. At the Japan Fine Ceramics Center, he researched fabrication of an ultra-thin single crystal Si quantum well sandwiched between two Si dioxide layers using SIMOX technology. He is currently with the Nanoelectronics Laboratory, University of Cincinnati, Cincinnati, OH, as a Research Associate, where his focus is on the multiple color integration of RE-doped GaN ELDs. His research has resulted in over 10 publications.

Robert Jones received the B.S. degree in physics from the University of South Florida, Tampa, FL, and the M.S. degree in physics from the University of Cincinnati, Cincinnati, OH, in 1998 and 2001, respectively. His undergraduate work focused on thin film growth by dual laser ablation for solar cell applications, while his graduate work focused on the optical properties of CdSe self assembled quantum dots.

In 2001, he joined the Nanoelectronics Laboratory, the University of Cincinnati, as a Research Associate and is currently involved in rare-earth-doped GaN phosphors grown by MBE on amorphous substrates and optimization of rare-earth-doped GaN electroluminescent device structures for flat-panel display applications. He has presented several formal presentations including at the American Physical Society National Meeting in March, 2001.

Mr. Jones is a member of the American Physical Society, Sigma Pi Sigma Physics Honor Society, and the Society for Information Display.